On mechanically induced degradation of fiber-reinforced hyperelastic materials

Seungik Baek and Thomas J. Pence

Mathematics and Mechanics of Solids 2011 16: 406 originally published online 7 April 2011
DOI: 10.1177/1081286511404040

Article

MMS

Mathematics and Mechanics of Solids
16(4): 406–434

DOI: 10.1177/1081286511404040
mms.sagepub.com

SAGE

On mechanically induced degradation of fiber-reinforced hyperelastic materials

Seungik Baek and Thomas J. Pence
Department of Mechanical Engineering, Michigan State University, East Lansing, MI, USA

Received 2 August 2010; accepted 11 October 2010

Abstract
A finite strain model for the mechanical degradation of composite materials with multiple families of fine reinforcing fibers is developed and studied. At any instant of time the matrix material may or may not be degrading with all, some, or none of the interpenetrating fibers also undergoing degradation. This multi-component description of damage is governed by coupled differential equations when more than one damage mechanism is active. These differential equations, and the threshold values of the strain invariants that activate the damage process, emerge naturally from a general framework that describes the response of dissipative systems under a maximum rate of dissipation postulate. In this context we then study uniaxial loadings when either a constant stretch or a constant force is suddenly applied to the composite. It is found that the initial type of degradation (e.g. degrading fibers in a non-degrading matrix) may transition to an alternative type of degradation (e.g. the degradation of all constituents) at some finite time into the process. A rich variety of material and load-dependent transition possibilities are systematically uncovered using a combination of asymptotic and numerical techniques. The resulting macroscopic behavior as the material weakens involves relaxation and creep phenomena that are formally similar to viscoelastic material behavior in solids even though the underlying processes are significantly different. Describing implants and tissue constructs containing biodegradable polymers is one possible area of application.

Keywords
biodegradable constructs, constitutive behavior, creep, degradable polymer, fiber-reinforced materials, hyperelasticity, maximum rate of dissipation, stress relaxation

1. Introduction

Degradable polymers are macromolecules which structurally degrade when subject to a variety of external stimuli including, as determined by the material system in question: moisture, temperature, corrosion agents, and even light exposure. These degradation processes are typically accelerated when the material is either highly stressed or highly strained (e.g. [1, 2]). The degradation itself may involve a variety of damage mechanisms. For polymer matrices containing polymeric fibers these degradation mechanisms include scission of the long-chain molecules comprising the matrix and dissolution of the internal filaments comprising the structural fibers. The modeling of large deformation mechanical degradation in single-component isotropic materials has been placed in a useful continuum mechanical framework in [3] using concepts from irreversible thermodynamics

Corresponding author:
Seungik Baek, Department of Mechanical Engineering, Michigan State University, East Lansing, MI 48824, USA
Email: sbaek@egr.msu.edu

(namely [4]). In [3] it is shown how a maximum rate of dissipation postulate can lead to a single differential equation that governs the time evolution of a damage variable which is a central ingredient of the constitutive description. Such a theory for example applies to isotropic polymers, that is, polymers that do not contain fiber reinforcement.

In the framework of [3] each point in the material may or may not be degrading as determined by the current local conditions of finite strain. At those locations where degradation is *not* currently taking place the material is instantaneously behaving as a classical hyperelastic material [5, 6]. In contrast, at locations where degradation is taking place the material is formally time dependent with structural mechanical properties that weaken with time. As described in [3], this degradation is dependent upon the local state of finite strain, with damage taking place at a faster rate at those locations where the strain measures which govern the damage are relatively greater. Such inhomogeneity in degradation kinetics of a degradable isotropic cylindrical annulus has been studied for various loading conditions in [7].

While the discussion in [3] places the phenomena under consideration in a wide physical context, the mathematical framework as developed in detail in [3] limits attention to the consideration of isotropic materials under considerations of purely mechanical degradation as determined by elevated states of strain. In the present paper we maintain the purely mechanical focus of [3] while generalizing the class of materials under consideration so as to allow for directional stiffening in key directions. In particular, this allows for the consideration of degradation of fiber–matrix composites. For such materials it is then necessary to consider the various possibilities in which all, some or none of the individual fiber and matrix constituents may be undergoing degradation at any instant of time. When no degradation is taking place in any of the constituents, that is, when all of the structural components maintain fixed mechanical properties, then the framework described here reduces to a conventional anisotropic hyperelastic theory. Such overall material stability can be lost, meaning that the material suffers degradation, when various finite strain measures exceed threshold values. As in [3] these threshold values emerge naturally from the theoretical treatment. However, unlike the particular theory developed in [3], the presence of multiple structural components (i.e. a matrix containing possibly multiple families at fibers) at each material point in the present continuum description allows for the possibility that multiple degradation mechanisms can be occurring simultaneously at each material point. Mathematically, this leads to a multicomponent description of damage that is in turn governed by coupled differential equations whenever more than one damage mechanism is active.

In the present paper we consider the case where the material contains two families of reinforcing fibers that proceed through the material at sufficiently fine scales so as to be amenable to a continuum description at each material point. In particular, this allows for the consideration of various fine-scale 'cross-ply' and 'woven fabric' types of reinforcing. Our previously stated focus on purely mechanical effects means that we do not here seek to account for hygrothermal, chemical, or radiation effects, although the broader consideration of how such agents would couple to the purely mechanical stress–deformation phenomena considered here is certainly of significant interest and hence is motivation for future examination in the context of a suitably generalized version of the present treatment. Here we remark that we have recently considered the possibility of swelling induced degradation of a fiber reinforced material using similar concepts [8],[1] where attention was restricted to transverse isotropy, i.e. the case of a single reinforcing direction. The present paper, while not considering the issue of swelling, develops the framework of [3] and [8] so as to apply to a relatively general class of fiber-reinforced materials. In the process we uncover a variety of interesting damage-induced creep and relaxation effects due to material weakening that were not readily apparent from such earlier studies.

We begin in the next section with the underlying thermodynamic framework which in the present purely mechanical setting makes use of two basic constitutive functions: a Helmholtz stored energy density W, and a rate of mechanical energy dissipation function $\hat{\xi}$. Degradation of the matrix and the two fiber families is encapsulated in three scalar variables: α_m, α_{f_1}, and α_{f_2}, respectively, each of which increases when there is degradation of the associated material constituent. The maximum rate of dissipation postulate then leads to general expressions for the Cauchy stress $\mathbf{T}$ and to basic conditions governing the time evolution of the degradation scalars. Special classes of constitutive functions W and $\hat{\xi}$ are introduced in Section 3 so as to represent the fiber–matrix composites of interest. Here it is useful to remark that the hyperelastic modeling of such materials is currently a subject of considerable interest (namely, [14, 15, 16, 17, 18]) and, in particular, such models are receiving

increasing attention in the modeling of biological soft tissue (namely, [19, 20, 21]). The modeling presented here then results in eight separate possible degradation cases, as determined by which of the three constituents are degrading in conjunction with each other (including the trivial case of no degradation). Each of the seven nontrivial degradation cases is governed by appropriate kinetic evolution equations for the increase of either α_m, α_{f_1}, or α_{f_2}.

The theory is illustrated in the context of homogeneous deformations involving uniaxial loading. By considering loading that is symmetric with respect to the two fiber families, attention is restricted to degradation that proceeds equally in the two fiber families. As indicated in Section 4 this reduces from eight to four the number of separate degradation cases which must be considered. These ideas are developed in the context of a degradation phase diagram whose axes are the two principal stretches in the fiber-containing plane. The form of these phase diagrams is dependent upon the material parameters that enter into the constitutive functions W and $\hat{\xi}$. Hard (isometric) loading is examined in Section 5 wherein the axial stretch is fixed. Degradation then gives rise to paths in the phase diagram and, depending on the intensity of the applied stretch, the degradation path may pass through different regions of the phase diagram corresponding to different types of degradation. In all cases, degradation gives rise to a stress relaxation type of phenomenon when the axial stretch is fixed. In contrast, if the overall force is fixed, then a creep-type phenomenon is observed as the material degrades. The associated soft (isotonic) loading is examined in Section 6. More complex degradation paths are generated for isotonic loading than are generated for isometric loading since now both stretch components may change with time. Even so, the basic qualitative features of the mechanical response can be determined directly from analytical arguments based upon the asymptotics of the governing ordinary differential equations (ODEs). These results are confirmed directly by separate numerical simulation. Indeed a major focus of both Sections 5 and 6 involves the use of rigorous qualitative arguments that examine how degradation paths are attracted to particular asymptotic state curves in the degradation phase diagram. The paper concludes with summary comments in Section 7 including the particular relevance of this study to biodegradable polymers.

2. Kinematics and thermodynamic framework

Let $\mathbf{X}$ be the position vector of a typical particle in the reference configuration that is regarded as the state of the unloaded body prior to degradation. Locations in the deformed body are denoted by $\mathbf{x}$. The deformation is an invertible mapping from $\mathbf{X}$ to $\mathbf{x}$. The deformation gradient is $\mathbf{F} = \partial\mathbf{x}/\partial\mathbf{X}$. The left and right Cauchy–Green deformation tensors are defined by

$$\mathbf{B} = \mathbf{F}\mathbf{F}^{\mathrm{T}}, \quad \mathbf{C} = \mathbf{F}^{\mathrm{T}}\mathbf{F}.$$

Let $\mathbf{v}$ be the particle velocity vector, and $\mathbf{L}$ and $\mathbf{D}$ denote the velocity gradient tensor and the stretching tensor, respectively, i.e.

$$\mathbf{v} = \frac{\partial \mathbf{x}}{\partial t} = \dot{\mathbf{x}}, \quad \mathbf{L} = \dot{\mathbf{F}}\mathbf{F}^{-1}, \quad \mathbf{D} = \frac{1}{2}(\mathbf{L} + \mathbf{L}^{\mathrm{T}}), \tag{1}$$

where a superposed dot denotes time differentiation while holding the particle fixed.[2]

The material is taken to be incompressible so that $\mathbf{F}$ is subject to the constraint

$$\det\mathbf{F} = 1. \tag{2}$$

We consider a material with two families of fibers. Unit vectors $\mathbf{M}^{(1)}$ and $\mathbf{M}^{(2)}$ give the orientation of these fibers in the reference configuration of the composite material. In general, these directions could vary with location $\mathbf{X}$, and each family is subject to the possibility of degradation. Individual fibers are not spatially resolved in this continuum treatment so that their presence is accounted for by the anisotropic constitutive law of the material.

The Cauchy stress field is denoted by $\mathbf{T}$ and is subject to the usual stress equations of equilibrium

$$\mathrm{div}\,\mathbf{T} = \mathbf{0}.$$

Degradation is described by means of the scalar field variables α_m, α_{f_1}. and α_{f_2} which represent the respective degree of degradation of the matrix and of the two fiber families at the reference location $\mathbf{X}$ at time t. The values

$\alpha_m = 0$ and $\alpha_{f_i} = 0$, $i = 1, 2$, denote the undamaged material state, whereas the values $\alpha_m = 1$ and $\alpha_{f_i} = 1$ represent full degradation. It is assumed that both α_m and the α_{f_i} cannot decrease with time, hence it is required that

$$\dot{\alpha}_m \geq 0, \quad \dot{\alpha}_{f_i} \geq 0 \quad (i = 1, 2). \tag{3}$$

In particular, there is no notion of healing in the present development. Degradation occurs at those instants of time at which at least one of the inequalities in Equation (3) is strict. Since $\alpha_m = \alpha_m(\mathbf{X}, t)$, $\alpha_{f_1} = \alpha_{f_1}(\mathbf{X}, t)$ and $\alpha_{f_2} = \alpha_{f_2}(\mathbf{X}, t)$ it can be the case that degradation occurs at some material points but not at other material points.

Attention is restricted to isothermal processes so that temperature need not enter into the formal development. For the temperature of interest let W be the Helmholtz energy density of the fiber–matrix composite per unit volume in the reference configuration. It is a function of $\mathbf{C}$ and the degree of degradation of each constituent and so is written as

$$W = W(\mathbf{C}, \alpha_m, \alpha_{f_1}, \alpha_{f_2}).$$

The rate of mechanical energy dissipation ξ is the difference between the stress power and the rate of change in the mechanical energy storage. The second law statement of continuum thermodynamics for isothermal processes then reduces to a requirement that this dissipation is non-negative. This is expressed as

$$\xi := \mathbf{T} : \mathbf{D} - \dot{W} \geq 0. \tag{4}$$

Although the thermodynamic framework employed in this work is general enough to include diffusion and chemical reactions of chemical species with the functional groups in a macromolecule network (e.g. [22]), our concern here is modeling of degradation processes induced by finite strain and it is assumed for the present development that the degradation processes are the only source of dissipation. As in [3] the functional form for ξ is specified constitutively:

$$\xi = \hat{\xi}(\mathbf{C}, \alpha_m, \alpha_{f_1}, \alpha_{f_2}, \dot{\alpha}_m, \dot{\alpha}_{f_1}, \dot{\alpha}_{f_2}). \tag{5}$$

By the maximum rate of dissipation formalism [3] it is assumed that the degradation processes of interest proceed so as to maximize this quantity.

Evaluating $\dot{W}$ with the aid of the chain rule allows Equation (4) to be expressed as

$$\left(\mathbf{T} - 2\mathbf{F}\frac{\partial W}{\partial \mathbf{C}}\mathbf{F}^{\mathrm{T}}\right) : \mathbf{D} - \frac{\partial W}{\partial \alpha_m}\dot{\alpha}_m - \frac{\partial W}{\partial \alpha_{f_1}}\dot{\alpha}_{f_1} - \frac{\partial W}{\partial \alpha_{f_2}}\dot{\alpha}_{f_2} = \xi. \tag{6}$$

The rate form of the constraint (2) is $\mathbf{D} : \mathbf{I} = 0$. Thus, maximizing ξ subject to (5), (6), and $\mathbf{D} : \mathbf{I} = 0$ gives, by means of the two Lagrange multipliers λ_1 and λ_2, the following auxiliary function

$$\Phi = \hat{\xi} - \lambda_1\left(\left(\mathbf{T} - 2\mathbf{F}\frac{\partial W}{\partial \mathbf{C}}\mathbf{F}^{\mathrm{T}}\right) : \mathbf{D} - \frac{\partial W}{\partial \alpha_m}\dot{\alpha}_m - \frac{\partial W}{\partial \alpha_{f_1}}\dot{\alpha}_{f_1} - \frac{\partial W}{\partial \alpha_{f_2}}\dot{\alpha}_{f_2} - \hat{\xi}\right) - \lambda_2\mathbf{D} : \mathbf{I}.$$

The extrema of Φ with respect to $\mathbf{D}$ is found by requiring that the derivative of Φ with respect to $\mathbf{D}$ vanishes; this gives

$$-\lambda_1\left(\mathbf{T} - 2\mathbf{F}\frac{\partial W}{\partial \mathbf{C}}\mathbf{F}^{\mathrm{T}}\right) - \lambda_2\mathbf{I} = 0. \tag{7}$$

In view of (3) the extrema of Φ with respect to $\dot{\alpha}_m$ requires either that $\dot{\alpha}_m = 0$ or otherwise that the derivative of Φ with respect to $\dot{\alpha}_m$ vanishes, the latter of which gives

$$\frac{\partial \hat{\xi}}{\partial \dot{\alpha}_m} + \lambda_1\left(\frac{\partial W}{\partial \alpha_m} + \frac{\partial \hat{\xi}}{\partial \dot{\alpha}_m}\right) = 0. \tag{8}$$

Similarly, either $\dot{\alpha}_{f_1} = 0$ or otherwise

$$\frac{\partial \hat{\xi}}{\partial \dot{\alpha}_{f_1}} + \lambda_1\left(\frac{\partial W}{\partial \alpha_{f_1}} + \frac{\partial \hat{\xi}}{\partial \dot{\alpha}_{f_1}}\right) = 0. \tag{9}$$

Finally, either $\dot{\alpha}_{f_2} = 0$ or otherwise

$$\frac{\partial \hat{\xi}}{\partial \dot{\alpha}_{f_2}} + \lambda_1 \Big(\frac{\partial W}{\partial \alpha_{f_2}} + \frac{\partial \hat{\xi}}{\partial \dot{\alpha}_{f_2}} \Big) = 0. \tag{10}$$

On the assumption that $\lambda_1 \neq 0$, conditions (7)–(10) give

$$\mathbf{T} = 2\mathbf{F}\frac{\partial W}{\partial \mathbf{C}}\mathbf{F}^{\mathrm{T}} - p\mathbf{I}, \tag{11}$$

$$-\frac{\partial W}{\partial \alpha_m} = \eta \frac{\partial \hat{\xi}}{\partial \dot{\alpha}_m} \quad (\text{if } \dot{\alpha}_m > 0), \tag{12}$$

$$-\frac{\partial W}{\partial \alpha_{f_1}} = \eta \frac{\partial \hat{\xi}}{\partial \dot{\alpha}_{f_1}} \quad (\text{if } \dot{\alpha}_{f_1} > 0), \tag{13}$$

$$-\frac{\partial W}{\partial \alpha_{f_2}} = \eta \frac{\partial \hat{\xi}}{\partial \dot{\alpha}_{f_2}} \quad (\text{if } \dot{\alpha}_{f_2} > 0), \tag{14}$$

where $p = \lambda_2/\lambda_1$ and $\eta = (1 + \lambda_1)/\lambda_1$. Substituting from (11) back into (6) and using the constraint $\mathbf{D} : \mathbf{I} = 0$ gives

$$\hat{\xi} = -\frac{\partial W}{\partial \alpha_m}\dot{\alpha}_m - \frac{\partial W}{\partial \alpha_{f_1}}\dot{\alpha}_{f_1} - \frac{\partial W}{\partial \alpha_{f_2}}\dot{\alpha}_{f_2}. \tag{15}$$

By virtue of (12)–(14) this can also be written as

$$\hat{\xi} = \eta \frac{\partial \hat{\xi}}{\partial \dot{\alpha}_m}\dot{\alpha}_m + \eta \frac{\partial \hat{\xi}}{\partial \dot{\alpha}_{f_1}}\dot{\alpha}_{f_1} + \eta \frac{\partial \hat{\xi}}{\partial \dot{\alpha}_{f_2}}\dot{\alpha}_{f_2}$$

from which one obtains that

$$\eta = \frac{\hat{\xi}}{\frac{\partial \hat{\xi}}{\partial \dot{\alpha}_m}\dot{\alpha}_m + \frac{\partial \hat{\xi}}{\partial \dot{\alpha}_{f_1}}\dot{\alpha}_{f_1} + \frac{\partial \hat{\xi}}{\partial \dot{\alpha}_{f_2}}\dot{\alpha}_{f_2}}. \tag{16}$$

The rate equation (15) shows how, in this framework, all of the mechanical dissipation is associated with degradation of either the matrix or the fiber constituents. In this regard the separate driving forces for matrix and fiber degradation are identified as

$$D_m = -\frac{\partial W}{\partial \alpha_m}, \qquad D_{f_1} = -\frac{\partial W}{\partial \alpha_{f_1}}, \qquad D_{f_2} = -\frac{\partial W}{\partial \alpha_{f_2}}. \tag{17}$$

3. Specific forms for the constitutive functions

We continue the development in the context of particular expressions for the elastic strain energy W and specific functional forms for the dissipation $\hat{\xi}$.

3.1. Elastic strain energy functions with degradation-dependent constitutive parameters

Standard models in hyperelasticity are readily generalized to account for degradation by allowing the constitutive parameters to 'weaken'. To this end let W be given by

$$W(\mathbf{C}, \alpha_m, \alpha_{f_1}, \alpha_{f_2}) = \frac{1}{2}\mu(I_1 - 3) + \frac{1}{2}\gamma_1(I_4^{(1)} - \lambda_{nat_1}^2)^2 + \frac{1}{2}\gamma_2(I_4^{(2)} - \lambda_{nat_2}^2)^2, \tag{18}$$

where

$$I_1 = \mathrm{tr}\mathbf{C} = \mathbf{F} : \mathbf{F}, \tag{19}$$

$$I_4^{(1)} = \mathbf{M}^{(1)} \cdot \mathbf{CM}^{(1)} = \mathbf{FM}^{(1)} \cdot \mathbf{FM}^{(1)}, \tag{20}$$

$$I_4^{(2)} = \mathbf{M}^{(2)} \cdot \mathbf{CM}^{(2)} = \mathbf{FM}^{(2)} \cdot \mathbf{FM}^{(2)}. \tag{21}$$

In the absence of damage, this W with $\gamma_2 = 0$ and $\lambda_{nat_1} = 1$ is a simple and relatively standard material model for a neo-Hookean material that is reinforced with a single family of aligned fibers that are at their natural length in the reference configuration. The generalization to $\gamma_2 \neq 0$ with $\lambda_{nat_2} = 1$ allows for the consideration of two such fiber families. More generally, λ_{nat_i} is a material parameter that allows for the consideration of fiber pre-stretch in the i fiber family. For example, λ_{nat_1} is the stretch that puts a fiber from fiber family 1 into its natural length in the reference configuration. If the fiber is at its natural length in the reference configuration, then $\lambda_{nat_1} = 1$.

The strain energy W given by (18) contains moduli μ, γ_1 and γ_2. These moduli are allowed to depend upon the current state of degradation by relations of the form

$$\mu = \hat{\mu}(\alpha_m), \quad \gamma_1 = \hat{\gamma}_1(\alpha_{f_1}), \quad \gamma_2 = \hat{\gamma}_2(\alpha_{f_2}), \tag{22}$$

where $\hat{\mu}$, $\hat{\gamma}_1$, and $\hat{\gamma}_2$ are constitutive functions. This accounts for the presence of α_m and α_{f_i} in the argument list of W in Equation (18). The functions $\hat{\mu}$, $\hat{\gamma}_1$, and $\hat{\gamma}_2$ remain constant as long as α_m and α_{f_i} remain constant, in which case Equation (18) is a simple, but standard, model for a hyperelastic material that is anisotropic by virtue of fiber reinforcement [23].

If the fibers in the two families are distinguished only by different directions but are otherwise the same as regards their mechanical properties and the way in which degradation affects these properties, then $\lambda_{nat_1} = \lambda_{nat_2} \equiv \lambda_{nat}$ and

$$\gamma_1 = \hat{\gamma}(\alpha_{f_1}), \qquad \gamma_2 = \hat{\gamma}(\alpha_{f_2}), \tag{23}$$

where the single function $\hat{\gamma}(\cdot)$ now replaces the previously separate functions $\hat{\gamma}_1(\cdot)$ and $\hat{\gamma}_2(\cdot)$. We henceforth assume that γ_1 and γ_2 are governed by relations of the form (23) in what follows.

The stress tensor $\mathbf{T}$ which then follows from (11) and (18) under these assumptions is

$$\mathbf{T} = -p\mathbf{I} + \mu\mathbf{B} + 2\gamma_1(I_4^{(1)} - \lambda_{nat}^2)\mathbf{FM}^{(1)} \otimes \mathbf{FM}^{(1)} + 2\gamma_2(I_4^{(2)} - \lambda_{nat}^2)\mathbf{FM}^{(2)} \otimes \mathbf{FM}^{(2)}. \tag{24}$$

The stress in the reference configuration is then found by taking $\mathbf{F} = \mathbf{I}$ and hence $\mathbf{C} = \mathbf{I}$, $I_4^{(1)} = I_4^{(2)} = 1$ so that Equation (24) reduces to

$$\mathbf{T} = (-p + \mu)\mathbf{I} + 2(1 - \lambda_{nat}^2)\Big(\gamma_1\mathbf{M}^{(1)} \otimes \mathbf{M}^{(1)} + \gamma_2\mathbf{M}^{(2)} \otimes \mathbf{M}^{(2)}\Big). \tag{25}$$

Thus, if $\lambda_{nat} = 1$, then the undeformed configuration is stress free upon taking $p = \mu$. However, if $\lambda_{nat} \neq 1$, then the condition $\mathbf{T} = \mathbf{0}$ cannot be met by Equation (25) for any choice of p. This is to expected since $\lambda_{nat} \neq 1$ corresponds to fibers that are prestressed with respect to the reference configuration.

While the consideration of initially prestressed fibers is of significant interest, the most essential features of the present modeling are most easily illustrated in the context of a composite material for which all of the fiber families are at their natural length in the reference configuration. Since this case is of substantial physical interest in its own right, we subsequently limit attention to the case $\lambda_{nat} = 1$ for the rest of this paper. That is, we henceforth take a simplification of Equation (18) in the form of

$$W(\mathbf{C}, \alpha_m, \alpha_{f_1}, \alpha_{f_2}) = \frac{1}{2}\mu(I_1 - 3) + \frac{1}{2}\gamma_1(I_4^{(1)} - 1)^2 + \frac{1}{2}\gamma_2(I_4^{(2)} - 1)^2. \tag{26}$$

The Cauchy stress which now follows on the basis of (11) is then

$$\mathbf{T} = -p\mathbf{I} + \mu\mathbf{B} + 2\gamma_1(I_4^{(1)} - 1)\mathbf{FM}^{(1)} \otimes \mathbf{FM}^{(1)} + 2\gamma_2(I_4^{(2)} - 1)\mathbf{FM}^{(2)} \otimes \mathbf{FM}^{(2)}. \tag{27}$$

Degradation is associated with a decrease in value of the moduli μ, γ_1 or γ_2 as given by Equations $(22)_1$ and (23). A simple model that we will consider here is (see [8])

$$\hat{\mu}(\alpha_m) = \mu_0(1 - \beta_m\alpha_m), \qquad \hat{\gamma}(\alpha_f) = \gamma_0(1 - \beta_f\alpha_f), \tag{28}$$

where we have used the generic placeholder variable α_f for the purposes of giving $\hat{\gamma}$. In Equation (28), β_m and β_f are material constants obeying $0 < \beta_m \leq 1$ and $0 < \beta_f \leq 1$. Also μ_0 and γ_0 are the original modulus values for the undamaged material. The minimum value for the modulus functions, meaning that associated with either maximal matrix degradation or maximal fiber degradation, are respectively given by $\hat{\mu}(1) = (1 - \beta_m)\mu_0$ and $\hat{\gamma}(1) = (1 - \beta_f)\gamma_0$. Thus, β_m and β_f are constitutive parameters that represent the maximum possible degradation (with values closer to one meaning a larger possible maximum degradation, and a value of one meaning that the constituent deteriorates to the extent that it no longer offers any structural support).

It follows from Equation (17) that the specific forms (26) and (28) give degradation driving forces

$$D_m = \frac{\beta_m \mu_0}{2}(I_1 - 3) \geq 0, \tag{29}$$

$$D_{f_1} = \frac{\beta_f \gamma_0}{2}(I_4^{(1)} - 1)^2 \geq 0, \tag{30}$$

$$D_{f_2} = \frac{\beta_f \gamma_0}{2}(I_4^{(2)} - 1)^2 \geq 0. \tag{31}$$

3.2. A rate of dissipation function that is motivated by the isotropic form of Rajagopal et al.

We now turn to consider the second constitutive function that is central to the modeling, namely that which governs the dissipation ξ. To this end we take the rate of dissipation to be given as the sum of separately identifiable rates of dissipation for each of the three constituents: matrix, fiber family 1, and fiber family 2. Motivated by the form discussed by Rajagopal *et al.* in [3] consider

$$\hat{\xi} = \hat{\xi}_m(\alpha_m, \dot{\alpha}_m) + \hat{\xi}_f(\alpha_{f_1}, \dot{\alpha}_{f_1}) + \hat{\xi}_f(\alpha_{f_2}, \dot{\alpha}_{f_2}), \tag{32}$$

with

$$\hat{\xi}_m(\alpha_m, \dot{\alpha}_m) = \Gamma_m \dot{\alpha}_m + \Lambda_m \frac{(\dot{\alpha}_m)^{\frac{n_m+1}{n_m}}}{(1 - \alpha_m)^{\frac{1}{n_m}}}, \tag{33}$$

$$\hat{\xi}_f(\alpha_f, \dot{\alpha}_f) = \Gamma_f \dot{\alpha}_f + \Lambda_f \frac{(\dot{\alpha}_f)^{\frac{n_f+1}{n_f}}}{(1 - \alpha_f)^{\frac{1}{n_f}}}, \tag{34}$$

where Γ_m, Λ_m, n_m, Γ_f, Λ_f, n_f are positive material constants. It is to be noted that the same function $\hat{\xi}_f$ is taken to apply to both families of fibers so as to remain in keeping with the notion that each fiber family is identical with respect to its original mechanical properties. As indicated in what follows, the form of both $\hat{\xi}_m$ and $\hat{\xi}_f$ gives rise to a degradation threshold characterized by the first terms in each expression (namely that with the Γ_m and Γ_f), followed by a damage evolution which is governed by the second term.

3.3. Kinetic evolution ODEs for the degradation process

We now turn to consider the detailed kinetic relations governing the evolution of α_m, α_{f_1}, and α_{f_2} on the basis of the above development. In view of Equation (3) it follows that there are eight possibilities:

- no degradation (N): $\dot{\alpha}_m = 0, \dot{\alpha}_{f_1} = 0, \dot{\alpha}_{f_2} = 0$;
- matrix degradation only (M): $\dot{\alpha}_m > 0, \dot{\alpha}_{f_1} = 0, \dot{\alpha}_{f_2} = 0$;
- fiber family 1 degradation only (F1): $\dot{\alpha}_m = 0, \dot{\alpha}_{f_1} > 0, \dot{\alpha}_{f_2} = 0$;
- fiber family 2 degradation only (F2): $\dot{\alpha}_m = 0, \dot{\alpha}_{f_1} = 0, \dot{\alpha}_{f_2} > 0$;
- matrix degradation combined with degradation of the first fiber family (M1): $\dot{\alpha}_m > 0, \dot{\alpha}_{f_1} > 0, \dot{\alpha}_{f_2} = 0$;
- matrix degradation combined with degradation of the second fiber family (M2): $\dot{\alpha}_m > 0, \dot{\alpha}_{f_1} = 0, \dot{\alpha}_{f_2} > 0$;

- degradation of both fiber families (no matrix degradation) (FF): $\dot{\alpha}_m = 0, \dot{\alpha}_{f_1} > 0, \dot{\alpha}_{f_2} > 0$;
- degradation of all constituents (MFF): $\dot{\alpha}_m > 0, \dot{\alpha}_{f_1} > 0, \dot{\alpha}_{f_2} > 0$.

Consider the case M of matrix degradation. The associated kinetic equation for the matrix degradation emerges from (15) using $(17)_1$, (32)–(33), and $\dot{\alpha}_{f_1} = \dot{\alpha}_{f_2} = 0$. Algebraic manipulation then gives an equation of the general form treated in [3]:

$$\dot{\alpha}_m = \left(\frac{D_m - \Gamma_m}{\Lambda_m}\right)^{n_m}(1 - \alpha_m), \qquad \text{(M)}. \tag{35}$$

Since $\dot{\alpha}_m > 0$, it follows that this situation applies only if $D_m > \Gamma_m$, or equivalently (see (29))

$$I_1 > \frac{2\Gamma_m}{\beta_m \mu_0} + 3. \tag{36}$$

Turning to the case F1, one similarly obtains the kinetic equation

$$\dot{\alpha}_{f_1} = \left(\frac{D_{f_1} - \Gamma_f}{\Lambda_f}\right)^{n_f}(1 - \alpha_{f_1}), \qquad \text{(F1)}, \tag{37}$$

whereupon $\dot{\alpha}_{f_1} > 0$ requires that $D_{f_1} > \Gamma_f$. This will occur if

$$I_4^{(1)} > 1 + \sqrt{\frac{2\Gamma_f}{\beta_f \gamma_0}}, \tag{38}$$

meaning that the fiber is sufficiently stretched. In addition, if $\sqrt{2\Gamma_f/\beta_f\gamma_0} < 1$, then fiber degradation also occurs if

$$I_4^{(1)} < 1 - \sqrt{\frac{2\Gamma_f}{\beta_f \gamma_0}}, \tag{39}$$

meaning that the fiber is sufficiently contracted. Corresponding results hold for the case F2, namely

$$\dot{\alpha}_{f_2} = \left(\frac{D_{f_2} - \Gamma_f}{\Lambda_f}\right)^{n_f}(1 - \alpha_{f_2}), \qquad \text{(F2)}, \tag{40}$$

with a requirement that either

$$I_4^{(2)} > 1 + \sqrt{\frac{2\Gamma_f}{\beta_f \gamma_0}}, \tag{41}$$

or

$$I_4^{(2)} < 1 - \sqrt{\frac{2\Gamma_f}{\beta_f \gamma_0}}. \tag{42}$$

It follows that the case M of matrix degradation occurs if condition (36) is met and all of the conditions: (38), (39), (41), (42) are not met. Similarly, the case F1 of fiber degradation in the first fiber family occurs if either condition (38) or (39) is met and conditions (36), (41), and (42) are all not met. Conditions associated with the case F2 follow similarly.

The degradation possibility M1 occurs if (36) and either of (38) or (39) are simultaneously met, while both (41) and (42) are not met. In this case (15) with $(17)_1$, $(17)_2$, (32)–(34), and $\dot{\alpha}_{f_2} = 0$ gives

$$(D_m - \Gamma_m)\dot{\alpha}_m + (D_{f_1} - \Gamma_f)\dot{\alpha}_{f_1} = \Lambda_m \frac{(\dot{\alpha}_m)^{\frac{n_m+1}{n_m}}}{(1 - \alpha_m)^{\frac{1}{n_m}}} + \Lambda_f \frac{(\dot{\alpha}_{f_1})^{\frac{n_f+1}{n_f}}}{(1 - \alpha_{f_1})^{\frac{1}{n_f}}}. \tag{43}$$

A second kinetic equation is required to close the system. Note in this case that Equation (16) is not sufficient to ensure that both Equations (12) and (13) hold. Thus, the required second kinetic equation is obtained by eliminating η between Equations (12) and (13). This yields

$$\frac{1}{D_{f_1}}\left(\Gamma_f + \Lambda_f(1+\frac{1}{n_f})\left(\frac{\dot{\alpha}_{f_1}}{1-\alpha_{f_1}}\right)^{\frac{1}{n_f}}\right) = \frac{1}{D_m}\left(\Gamma_m + \Lambda_m(1+\frac{1}{n_m})\left(\frac{\dot{\alpha}_m}{1-\alpha_m}\right)^{\frac{1}{n_m}}\right). \tag{44}$$

Hence, Equations (43) and (44) serve as two ODEs for the degradation kinetics at each point in the body where degradation type M1 takes place.

Governing equations for the cases M2 and FF follow by a similar logic. Thus, for the case M2 one has $\dot{\alpha}_{f_1} = 0$ with α_m and α_{f_2} determined on the basis of the two equations

$$(D_m - \Gamma_m)\dot{\alpha}_m + (D_{f_2} - \Gamma_f)\dot{\alpha}_{f_2} = \Lambda_m \frac{(\dot{\alpha}_m)^{\frac{n_m+1}{n_m}}}{(1-\alpha_m)^{\frac{1}{n_m}}} + \Lambda_f \frac{(\dot{\alpha}_{f_2})^{\frac{n_f+1}{n_f}}}{(1-\alpha_{f_2})^{\frac{1}{n_f}}}, \tag{45}$$

and

$$\frac{1}{D_{f_2}}\left(\Gamma_f + \Lambda_f(1+\frac{1}{n_f})\left(\frac{\dot{\alpha}_{f_2}}{1-\alpha_{f_2}}\right)^{\frac{1}{n_f}}\right) = \frac{1}{D_m}\left(\Gamma_m + \Lambda_m(1+\frac{1}{n_m})\left(\frac{\dot{\alpha}_m}{1-\alpha_m}\right)^{\frac{1}{n_m}}\right). \tag{46}$$

For the case FF one has $\dot{\alpha}_m = 0$ with α_{f_1} and α_{f_2} determined on the basis of the two equations

$$(D_{f_1} - \Gamma_f)\dot{\alpha}_{f_1} + (D_{f_2} - \Gamma_f)\dot{\alpha}_{f_2} = \Lambda_f \frac{(\dot{\alpha}_{f_1})^{\frac{n_f+1}{n_f}}}{(1-\alpha_{f_1})^{\frac{1}{n_f}}} + \Lambda_f \frac{(\dot{\alpha}_{f_2})^{\frac{n_f+1}{n_f}}}{(1-\alpha_{f_2})^{\frac{1}{n_f}}}, \tag{47}$$

and

$$\frac{1}{D_{f_1}}\left(\Gamma_f + \Lambda_f(1+\frac{1}{n_f})\left(\frac{\dot{\alpha}_{f_1}}{1-\alpha_{f_1}}\right)^{\frac{1}{n_f}}\right) = \frac{1}{D_{f_2}}\left(\Gamma_f + \Lambda_f(1+\frac{1}{n_f})\left(\frac{\dot{\alpha}_{f_2}}{1-\alpha_{f_2}}\right)^{\frac{1}{n_f}}\right). \tag{48}$$

The final case is that of degradation of all of the constituents (MFF). In this case Equation (15) with (17) and (29) gives

$$\begin{aligned}(D_m - \Gamma_m)\dot{\alpha}_m + (D_{f_1} - \Gamma_f)\dot{\alpha}_{f_1} + (D_{f_2} - \Gamma_f)\dot{\alpha}_{f_2} \\ = \Lambda_m \frac{(\dot{\alpha}_m)^{\frac{n_m+1}{n_m}}}{(1-\alpha_m)^{\frac{1}{n_m}}} + \Lambda_f \frac{(\dot{\alpha}_{f_1})^{\frac{n_f+1}{n_f}}}{(1-\alpha_{f_1})^{\frac{1}{n_f}}} + \Lambda_f \frac{(\dot{\alpha}_{f_2})^{\frac{n_f+1}{n_f}}}{(1-\alpha_{f_2})^{\frac{1}{n_f}}}.\end{aligned} \tag{49}$$

It is now the case that two additional kinetic equations are required to close the system. In this case all of the quantities $\dot{\alpha}_m$, $\dot{\alpha}_{f_1}$, and $\dot{\alpha}_{f_2}$ are non-zero, whereupon it is required that the three conditions (12)–(14) all hold for the value of η as given by (16). Thus, one such condition follows as in the case M1 by eliminating η between (12) and (13) so as to again obtain (44). Similarly, another independent condition follows as in the case M2 by eliminating η between (12) and (14) so as to again obtain (46). Here we note that we could alternatively eliminate η between (13) and (14) so as to obtain (48). Any two of (44), (46), and (48) can be taken as the two closure conditions, since the unchosen third condition then follows from the other two.

This completes the specification of the degradation equations for the seven cases M–MFF. It is to be noted that the various governing differential equations (35), (37), (40), (43), (44), (45), (46), (47), (48), and (49) all contain either D_m, D_{f_1}, or D_{f_2} and so couple to the current state of deformation by virtue of (29)–(31). These issues will now be demonstrated in the context of uniaxial load.

4. Balanced uniaxial load

Suppose that the fibers are straight with properties that are independent of spatial location. The matrix material is also assumed to be independent of spatial location. If under these circumstances we consider homogenous deformation, then the Cauchy stress is independent of spatial position, so that the stress equations of equilibrium are automatically satisfied.

In the reference configuration, let $\mathbf{e}_3$ be a unit vector that is normal to the plane containing the two fiber families. We consider loadings that are consistent with states of plane stress in the fiber-containing plane.

Let the directions defined by the bisectors of the fiber alignment directions in the reference configuration be given by unit vectors $\mathbf{e}_1$ and $\mathbf{e}_2$ such that $\{\mathbf{e}_1, \mathbf{e}_2, \mathbf{e}_3\}$ is a right-handed system. That is to say we take

$$\mathbf{M}^{(1)} = \cos\Theta\mathbf{e}_1 + \sin\Theta\mathbf{e}_2 \tag{50}$$

$$\mathbf{M}^{(2)} = \cos\Theta\mathbf{e}_1 - \sin\Theta\mathbf{e}_2 \tag{51}$$

in terms of a given orientation angle Θ from $\mathbf{e}_1$ in the reference configuration.

Consider the case of balanced uniaxial loading with respect to the $\mathbf{e}_2$ axis, meaning that

$$\mathbf{T} = \begin{bmatrix} 0 & 0 & 0 \\ 0 & T & 0 \\ 0 & 0 & 0 \end{bmatrix}. \tag{52}$$

We seek the anticipated shear-free deformations, meaning that the deformation gradient is of the form

$$\mathbf{F} = \begin{bmatrix} \lambda_\perp & 0 & 0 \\ 0 & \lambda & 0 \\ 0 & 0 & \frac{1}{\lambda\lambda_\perp} \end{bmatrix} \tag{53}$$

so that λ is the axial stretch and $\lambda_\perp$ is the transverse stretch in the fiber-containing plane. Then

$$I_1 = \lambda_\perp^2 + \lambda^2 + \frac{1}{\lambda_\perp^2\lambda^2}, \tag{54}$$

$$I_4^{(1)} = I_4^{(2)} = \lambda_\perp^2\cos^2\Theta + \lambda^2\sin^2\Theta \equiv I_4. \tag{55}$$

It follows by virtue of the symmetry of the deformation that $\alpha_{f_1} = \alpha_{f_2} \equiv \alpha_f$ so that only symmetric degradation possibilities are assumed in this setting.[3]

Entering (27) with (50), (51), (53), (54), and (55), one finds, as required by (52), that $T_{12} = T_{13} = T_{23} = 0$, whereas the requirement $T_{33} = 0$ gives $p = \mu/\lambda_\perp^2\lambda^2$. Then the remaining conditions of $T_{11} = 0$, $T_{22} = T$ give

$$0 = \lambda_\perp^2 - \frac{1}{\lambda_\perp^2\lambda^2} + 4\frac{\gamma}{\mu}\left(\lambda_\perp^2\cos^2\Theta + \lambda^2\sin^2\Theta - 1\right)\lambda_\perp^2\cos^2\Theta, \tag{56}$$

$$T = \mu\left(\lambda^2 - \frac{1}{\lambda_\perp^2\lambda^2}\right) + 4\gamma\left(\lambda_\perp^2\cos^2\Theta + \lambda^2\sin^2\Theta - 1\right)\lambda^2\sin^2\Theta, \tag{57}$$

with $\mu = \hat{\mu}(\alpha_m)$ and $\gamma = \hat{\gamma}(\alpha_f)$ as given by (28).

The axial force needed to sustain this deformation is given by the product of T and the current cross-sectional area. The current cross-sectional area is the original area A_o multiplied by the two transverse stretches ($\lambda_\perp$ and $1/\lambda\lambda_\perp$). In other words the axial force is SA_o where

$$S = T/\lambda; \tag{58}$$

in fact, this S is the corresponding component of the Piola–Kirchhoff stress tensor. In this context we consider first a hard loading device and then a soft loading device.

For a *hard loading device*, the stretch λ is specified whereupon (56) – (58) determine $\lambda_\perp$, T and S. In the event that degradation occurs, as the material weakens one anticipates that a decreasing stress value S is sufficient to maintain the fixed value of λ. The time dependent stresses obtained on this basis exhibit a *stress relaxation*. The transverse stretch $\lambda_\perp$ would generally also exhibit change during this process as well.

For a *soft loading device*, the stress value S is specified whereupon (56)–(58) determine λ, $\lambda_\perp$, and T. In the event that degradation occurs, as the material weakens one anticipates that the fixed S gives an increasing stretch λ. The time-dependent stretch obtained on this basis would therefore exhibit a *creep elongation*. The changing λ in this process will in turn generally give rise to a changing $\lambda_\perp$ during this creep elongation.

It is to be remarked that hard loading (specified stretch) is sometimes referred to as *isometric* loading, and that soft loading (specified force) is sometimes referred to as *isotonic* loading.

4.1. Degradation scenarios

There are four possibilities consistent with the symmetry assumption $\alpha_{f_1} = \alpha_{f_2} \equiv \alpha_f$, namely N, M, FF or MFF. Furthermore, it follows from (36)–(42) that the values of λ and $\lambda_\perp$ completely determine the degradation type as follows:

- N occurs if λ and $\lambda_\perp$ obey

$$\lambda^2 + \lambda_\perp^2 + \frac{1}{\lambda^2\lambda_\perp^2} < 3 + \frac{2\Gamma_m}{\beta_m\mu_0},$$

and

$$-\sqrt{\frac{2\Gamma_f}{\beta_f\gamma_0}} < \lambda^2\sin^2\Theta + \lambda_\perp^2\cos^2\Theta - 1 < \sqrt{\frac{2\Gamma_f}{\beta_f\gamma_0}}.$$

  In this case both α_m and α_f do not change, so that the moduli μ and γ remain fixed. This includes the case $\lambda = \lambda_\perp = 1$ corresponding to no deformation.
- M occurs if λ and $\lambda_\perp$ obey

$$\lambda^2 + \lambda_\perp^2 + \frac{1}{\lambda^2\lambda_\perp^2} > 3 + \frac{2\Gamma_m}{\beta_m\mu_0},$$

and

$$-\sqrt{\frac{2\Gamma_f}{\beta_f\gamma_0}} < \lambda^2\sin^2\Theta + \lambda_\perp^2\cos^2\Theta - 1 < \sqrt{\frac{2\Gamma_f}{\beta_f\gamma_0}}.$$

  In this case α_f remains fixed, while the increase in α_m is governed by

$$t_m^*\dot{\alpha}_m = \left(\left(\lambda^2 + \lambda_\perp^2 + \frac{1}{\lambda^2\lambda_\perp^2} - 3\right) - \frac{2\Gamma_m}{\beta_m\mu_0}\right)^{n_m}(1 - \alpha_m).$$

  Here we have introduced a new constant

$$t_m^* = \left(\frac{2\Lambda_m}{\beta_m\mu_0}\right)^{n_m}, \tag{59}$$

  which is a natural time scale for the matrix degradation process.[4]
- FF occurs if λ and $\lambda_\perp$ obey

$$\lambda^2 + \lambda_\perp^2 + \frac{1}{\lambda^2\lambda_\perp^2} < 3 + \frac{2\Gamma_m}{\beta_m\mu_0},$$

and either

$$\lambda^2\sin^2\Theta + \lambda_\perp^2\cos^2\Theta - 1 > \sqrt{\frac{2\Gamma_f}{\beta_f\gamma_0}},$$

or

$$\lambda^2 \sin^2 \Theta + \lambda_\perp^2 \cos^2 \Theta - 1 < -\sqrt{\frac{2\Gamma_f}{\beta_f \gamma_0}}.$$

In this case α_m remains fixed, while it follows from Equation (47) that the increase in α_f is governed by

$$t_f^* \dot{\alpha}_f = \left(\left(\lambda^2 \sin^2 \Theta + \lambda_\perp^2 \cos^2 \Theta - 1\right)^2 - \frac{2\Gamma_f}{\beta_f \gamma_0}\right)^{n_f} (1 - \alpha_f), \tag{60}$$

where the time constant

$$t_f^* = \left(\frac{2\Lambda_f}{\beta_f \gamma_0}\right)^{n_f}, \tag{61}$$

is a natural time scale for the fiber degradation process. That Equation (60) is the sole evolution equation for the degradation in this case follows from the observation that Equation (48) is now satisfied identically.

- MFF occurs if λ and $\lambda_\perp$ obey

$$\lambda^2 + \lambda_\perp^2 + \frac{1}{\lambda^2 \lambda_\perp^2} > 3 + \frac{2\Gamma_m}{\beta_m \mu_0},$$

and either

$$\lambda^2 \sin^2 \Theta + \lambda_\perp^2 \cos^2 \Theta - 1 > \sqrt{\frac{2\Gamma_f}{\beta_f \gamma_0}},$$

or

$$\lambda^2 \sin^2 \Theta + \lambda_\perp^2 \cos^2 \Theta - 1 < -\sqrt{\frac{2\Gamma_f}{\beta_f \gamma_0}}.$$

In this case α_m and α_f simultaneously increase as governed by

$$\begin{aligned} &\left(\beta_m \mu_0 \left(\lambda^2 + \lambda_\perp^2 + \frac{1}{\lambda^2 \lambda_\perp^2} - 3\right) - 2\Gamma_m\right) \dot{\alpha}_m \\ &\quad + \left(2\beta_f \gamma_0 (\lambda^2 \sin^2 \Theta + \lambda_\perp^2 \cos^2 \Theta - 1)^2 - 4\Gamma_f\right) \dot{\alpha}_f \\ &\quad = \beta_m \mu_0 \frac{(t_m^* \dot{\alpha}_m)^{\frac{1}{n_m}} \dot{\alpha}_m}{(1 - \alpha_m)^{\frac{1}{n_m}}} + 2\beta_f \gamma_0 \frac{(t_f^* \dot{\alpha}_f)^{\frac{1}{n_f}} \dot{\alpha}_f}{(1 - \alpha_f)^{\frac{1}{n_f}}}, \end{aligned} \tag{62}$$

and

$$\begin{aligned} &\beta_m \mu_0 \left(\lambda^2 + \lambda_\perp^2 + \frac{1}{\lambda^2 \lambda_\perp^2} - 3\right) \left(\Gamma_f + \beta_f \gamma_0 \left(\frac{n_f + 1}{2n_f}\right) \left(\frac{t_f^* \dot{\alpha}_f}{1 - \alpha_f}\right)^{\frac{1}{n_f}}\right) \\ &= \beta_f \gamma_0 \left(\lambda^2 \sin^2 \Theta + \lambda_\perp^2 \cos^2 \Theta - 1\right)^2 \left(\Gamma_m + \beta_m \mu_0 \left(\frac{n_m + 1}{2n_m}\right) \left(\frac{t_m^* \dot{\alpha}_m}{1 - \alpha_m}\right)^{\frac{1}{n_m}}\right). \end{aligned} \tag{63}$$

We remark that the form of the kinetic equations listed above have eliminated the constitutive parameters Λ_m and Λ_f in terms of the characteristic degradation times t_m^* and t_f^*.

Table 1. Material parameters for two different materials.

	Θ	γ_o/μ_o	Γ_m/μ_o	Γ_f/μ_o	β_m	β_f
Material 1	$\pi/4$	0.5	0.08	0.001	0.8	0.6, 0.9, 1.0
Material 2	$\pi/4$	2.0	0.02	0.02	0.8	0.8

4.2. Degradation phase diagram

A degradation phase diagram of $(\lambda_\perp, \lambda)$ values obeying $\lambda_\perp > 0$ and $\lambda > 0$ is created by the separating curves from the above development. Namely the curves

$$\lambda^2 + \lambda_\perp^2 + \frac{1}{\lambda^2\lambda_\perp^2} = 3 + \frac{2\Gamma_m}{\beta_m\mu_0},$$

$$\lambda^2 \sin^2\Theta + \lambda_\perp^2 \cos^2\Theta = 1 + \sqrt{\frac{2\Gamma_f}{\beta_f\gamma_0}},$$

and, if $\beta_f\gamma_0 > 2\Gamma_f$, the curve

$$\lambda^2 \sin^2\Theta + \lambda_\perp^2 \cos^2\Theta = 1 - \sqrt{\frac{2\Gamma_f}{\beta_f\gamma_0}}, \tag{64}$$

separate regions of $(\lambda_\perp, \lambda)$-values corresponding to the four possibilities: N, M, FF, and MFF, thereby creating a *degradation phase diagram* for balanced uniaxial load. This diagram is dependent on the values of Θ, $\Gamma_m/\beta_m\mu_0$, and $\Gamma_f/\beta_f\gamma_0$.

For the purposes of illustration we consider two basic material parameter combinations in detail. Specifically, by *material 1* and *material 2* we mean material parameters: Θ, γ_0/μ_0, Γ_m/μ_0, Γ_f/μ_0, β_m, and β_f as shown in Table 1.

In Table 1 we use μ_0 as a normalization parameter for constitutive parameters with units of stress. For material 1 we shall consider three separate values of β_f as indicated in the table. We note that we do not specify Λ_m, Λ_f, n_m, and n_f for these materials. By virtue of Equations (59) and (61) this is the same as not specifying t_f^*, t_f^*, n_m, and n_f for these materials. In what follows we consider different values for these constants so as to clarify the affect of the degradation time scales.

Figure 1 shows the degradation phase diagram for material 1 with $\beta_f = 0.6$ while Figure 2 shows the degradation phase diagram for material 2. The phase diagram in Figure 1 shows degradation process zones for all four degradation types: N, M, FF, and MFF. In contrast, the phase diagram in Figure 2 does not admit to an FF degradation process. For both materials it is the case that $\beta_f\gamma_0 > 2\Gamma_f$ and the separating curve given by (64) is the inner circular arc in each diagram. Although not shown here, the phase diagram for material 1 with either $\beta_f = 0.9$ or $\beta_f = 1.0$ is similar in form to that in Figure 1. The only difference is that the larger values of β_f cause the two circular arcs to move closer together, which does not alter the basic form of the phase diagram in Figure 1.

Such a diagram is convenient for organizing the discussion of both the hard and the soft loading device. In each case we consider a step loading. For the hard device we consider a suddenly applied stretch $\lambda > 1$; for the soft device we consider a suddenly applied stress $S > 0$. The nature of the stress–stretch relations (56)–(58) then gives that $S > 0$ for the hard device, $\lambda > 1$ for the soft device, and $0 < \lambda_\perp < 1$ in both devices. The relations $\lambda > 1 \Leftrightarrow S > 0$ hold for all possible values of μ and γ obeying $0 < \mu \leq \mu_0$ and $0 < \gamma \leq \gamma_0$. Hence, for the ensuing discussion of step loading we may restrict attention to degradation phase diagrams on the region $0 < \lambda_\perp < 1$, $\lambda > 1$.

For each such diagram, Equation (56) with $\mu = \mu_0$ and $\gamma = \gamma_0$ determines the curve of uniaxial stretch states for an undamaged material. We call this the *curve of undamaged stretch states* and denote this curve by $\mathcal{C}_0$. For both the hard and soft loading device, the state of the system immediately after the application of load will be referred to as the initial state. All such initial states correspond to a point on the curve of undamaged

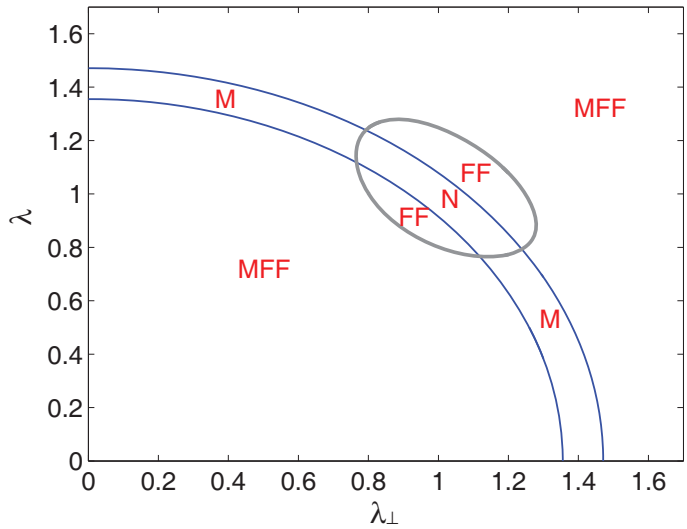

Figure 1. Degradation phase diagram for material 1 with β_f =0.6. Note that the undeformed location $(\lambda_\perp, \lambda) = (1,1)$ is in the N region where no degradation takes place.

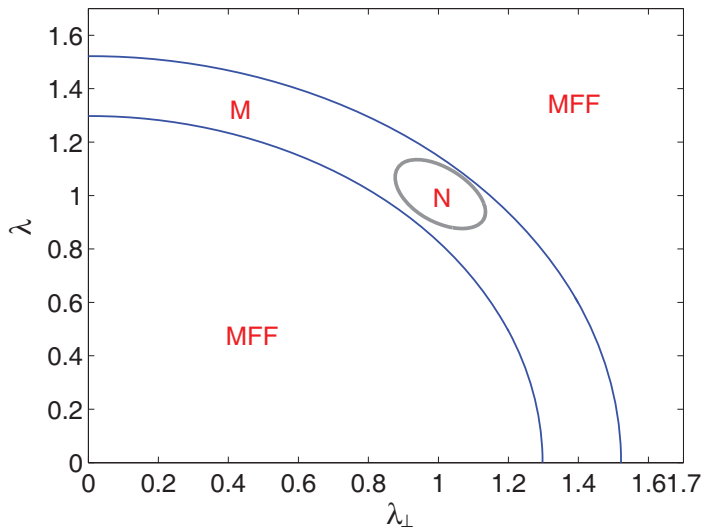

Figure 2. Degradation phase diagram for material 2. Once again the undeformed location $(\lambda_\perp, \lambda) = (1,1)$ is in the N region.

load states. However, if there is damage then, as time goes on, the value of $(\lambda_\perp, \lambda)$ will depart from this initial location. For the hard device, where λ is fixed, this departure will cause $(\lambda_\perp(t), \lambda)$ to trace out a horizontal path in the degradation phase diagram. For the soft device, where S is fixed, the trace of $(\lambda_\perp(t), \lambda(t))$ is a more general path. This will be demonstrated in detail in the examples that follow.

Before considering the path $(\lambda_\perp(t), \lambda(t))$ for any particular condition of soft or hard loading, it is useful to construct three additional load state curves analogous to the previously introduced curve of undamaged load states. These three additional curves are:

- the *curve of stretch states corresponding to full fiber degradation with an undamaged matrix*[5] that is obtained from Equation (56) upon setting $\mu = \mu_0$ and $\gamma = (1 - \beta_f)\gamma_0$; this curve will be denoted by $\mathcal{C}_\infty^{FF}$;

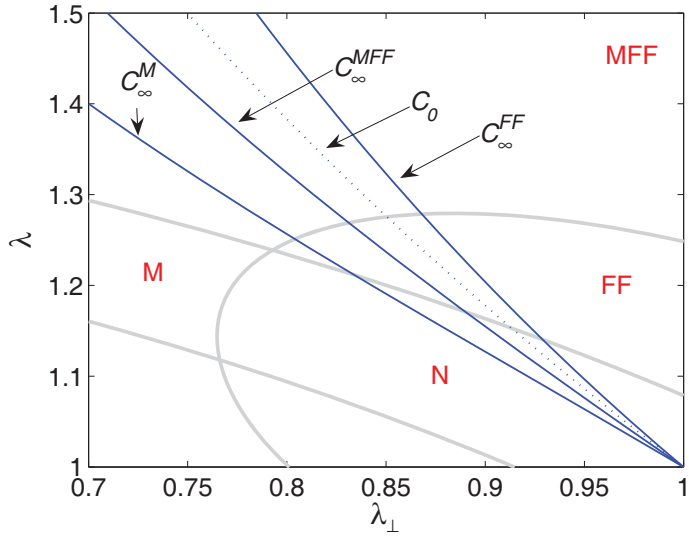

Figure 3. Degradation phase diagram for material 1 with $\beta_f = 0.6$ showing stretch state curves $\mathcal{C}_0$, $\mathcal{C}_\infty^M$, $\mathcal{C}_\infty^{FF}$, and $\mathcal{C}_\infty^{MFF}$.

- the *curve of stretch states corresponding to undamaged fibers with full matrix degradation* that is obtained from Equation (56) upon setting $\mu = (1 - \beta_m)\mu_0$ and $\gamma = \gamma_0$; this curve will be denoted by $\mathcal{C}_\infty^M$;
- the *curve of stretch states corresponding to full fiber degradation and full matrix degradation* that is obtained from Equation (56) upon setting $\mu = (1 - \beta_m)\mu_0$ and $\gamma = (1 - \beta_f)\gamma_0$; this curve will be denoted by $\mathcal{C}_\infty^{MFF}$.

These three curves, in conjunction with the curve of undamaged stretch states, each contain $(\lambda_\perp, \lambda) = (1, 1)$ and are otherwise completely determined by the different values of the ratio γ/μ. In the region $\lambda > 1$ of the degradation phase diagram these curves order themselves from left to right according to the value of the ratio γ/μ. In particular, the stretch state curve $\mathcal{C}_\infty^M$ is the leftmost such curve, and the stretch state curve $\mathcal{C}_\infty^{FF}$ is the rightmost such curve. As regards the ordering of the remaining two curves, it follows that the stretch state curve $\mathcal{C}_\infty^{MFF}$ is to the left of the curve of undamaged stretch states $\mathcal{C}_0$ if $\beta_f < \beta_m$, while $\mathcal{C}_\infty^{MFF}$ is to the right of $\mathcal{C}_0$ if $\beta_f > \beta_m$ (the two curves are coincident if $\beta_f = \beta_m$).

Figure 3 shows the degradation phase diagram for material 1 with $\beta_f = 0.6$ on the region $0 < \lambda_\perp \leq 1$, $\lambda \geq 1$ along with all four of the stretch state curves as discussed above. As already indicated, the initial $t = 0^+$ state of stretch for both the hard and soft loading device will correspond to a point on the curve $\mathcal{C}_0$. The other three stretch state curves are useful for describing the asymptotic state of stretch

$$(\lambda_\perp(\infty), \lambda(\infty)) \equiv \lim(\lambda_\perp(t), \lambda(t)), \qquad \text{as} \qquad t \to \infty.$$

Specifically, large time states in the MFF degradation region will asymptotically approach a point on the curve $\mathcal{C}_\infty^{MFF}$. The physical significance of the two curves $\mathcal{C}_\infty^M$ and $\mathcal{C}_\infty^{FF}$ is a bit more subtle. For example, if FF is the only type of degradation that has ever taken place then large time states in the FF degradation region will asymptotically approach a point on the curve $\mathcal{C}_\infty^{FF}$. Similarly, if M is the only type of degradation that has ever taken place then large time states in the M degradation region will asymptotically approach a point on the curve $\mathcal{C}_\infty^M$. In addition, the curves $\mathcal{C}_\infty^M$ and $\mathcal{C}_\infty^{FF}$ have significance in the MFF region as regards the possibility of an overshoot type phenomenon. These issues will now be illustrated in the context of particular examples for both the hard and the soft loading device.

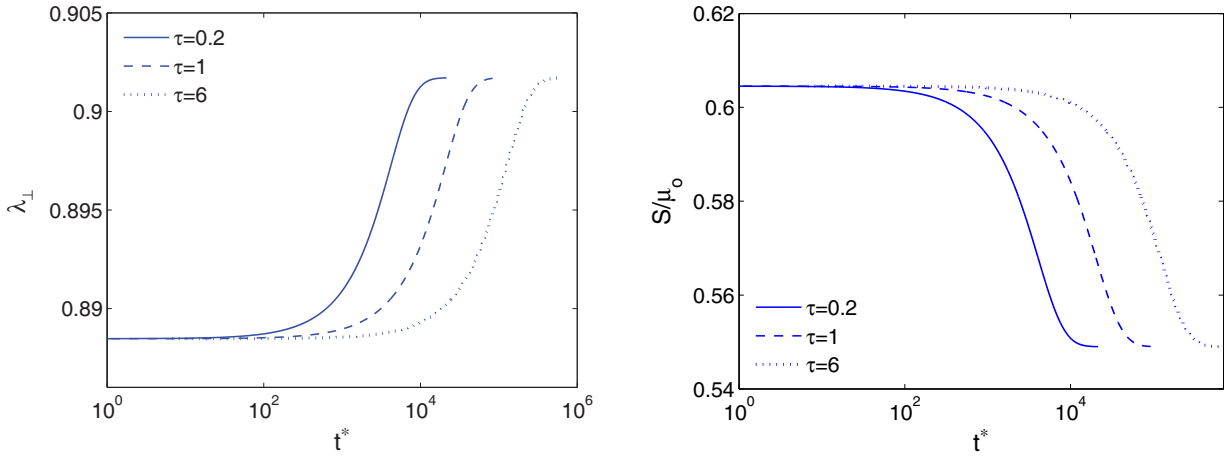

Figure 4. Transverse stretch $\lambda_\perp$ and nominal stress S/μ_o as a function of normalized time t^* for material I with $\beta_f = 0.6$. The case shown is of a hard loading device with $\lambda = 1.2$ so that the degradation is of type FF for all time. Here $n_f = n_m = 2$ and the non-dimensionalized time is defined by $t^* = t/t_m^*$. The three curves are for $\tau = 0.2$, 1, and 6.

5. Hard loading device

5.1. Material I with $\beta_f = 0.6$

Consider the hard loading device; a stretch $\lambda > 1$ is suddenly applied and subsequently held fixed. Our interest is in $S(t)$ and $\lambda_\perp(t)$. Using the specified value of λ it follows that the initial $t = 0^+$ value of $\lambda_\perp$ is immediate from the curve $\mathcal{C}_0$. Consider material 1 with $\beta_f = 0.6$ for which the degradation phase diagram is shown in Figure 3. This figure shows that the curve $\mathcal{C}_0$ is respectively within the N, FF, or MFF regions, according to whether $1 \le \lambda < 1.153$, $1.153 < \lambda < 1.275$, or $\lambda > 1.275$. This establishes the degradation type at $t = 0^+$ for the hard loading device. For example, the range $1 \le \lambda < 1.153$ gives no degradation and hence the material behaves as a conventional hyperelastic material. In this case both $\lambda_\perp$ and S remain at their initial $t = 0^+$ values for all time.

Suppose now that $1.153 < \lambda < 1.275$ so that the degradation type is initially FF. The subsequent increase in α_f is governed by (60) giving $\alpha_f \to 1$ as $t \to \infty$ and hence $\gamma \to (1 - \beta_f)\gamma_0 = 0.4\gamma_0$. The associated $t \to \infty$ value of $\lambda_\perp$ is therefore on the curve $\mathcal{C}_\infty^{FF}$. In the phase diagram of Figure 3 this curve is to the right of the curve of undamaged load states $\mathcal{C}_0$. As FF degradation proceeds, the time evolution of the pair $(\lambda_\perp(t), \lambda)$ generates a horizontal line segment on the phase diagram beginning on $\mathcal{C}_0$ and ending on $\mathcal{C}_\infty^{FF}$. Since this horizontal segment is confined to the FF region, the degradation remains of FF type for all time and the $t \to \infty$ state of the system, including both the $t \to \infty$ values of T and S, can be determined without solving the kinetic equation (60).

However, to consider the rate of the approach to the asymptotic values $\lambda_\perp(\infty)$ and $S(\infty)$ it is necessary to consider Equation (60) for the degradation kinetics. For FF degradation the degradation kinetics is dependent on the as yet unspecified value of t_f^*. To show the effect of different t_f^* it is convenient to normalize time by t_m^* and to introduce the non-dimensionalized parameter

$$\tau = \frac{t_f^*}{t_m^*} = \frac{(2\Lambda_f/\beta_f\gamma_o)^{n_f}}{(2\Lambda_m/\beta_m\mu_o)^{n_m}}.$$

Figure 4 shows curves of $\lambda_\perp$ versus t/t_m^* and S/μ_o versus t/t_m^* for $\lambda = 1.2$ with different values of τ. Larger values of τ correspond to a relatively longer time scale for the fiber degradation and hence a slower fiber degradation kinetics. This is confirmed in the figure where larger values of τ exhibit a slower approach to the asymptotic values $\lambda_\perp(\infty) = 0.902$ and $S(\infty) = 0.549\mu_0$. In all cases we find that this approach involves monotonic decrease from $S(0)$ to $S(\infty)$ confirming the anticipated stress relaxation.

In the context of the same phase diagram consider now the hard device loading when the degradation type is initially MFF, that is consider $\lambda > 1.275$. Then, as long as the degradation type remains MFF, the subsequent

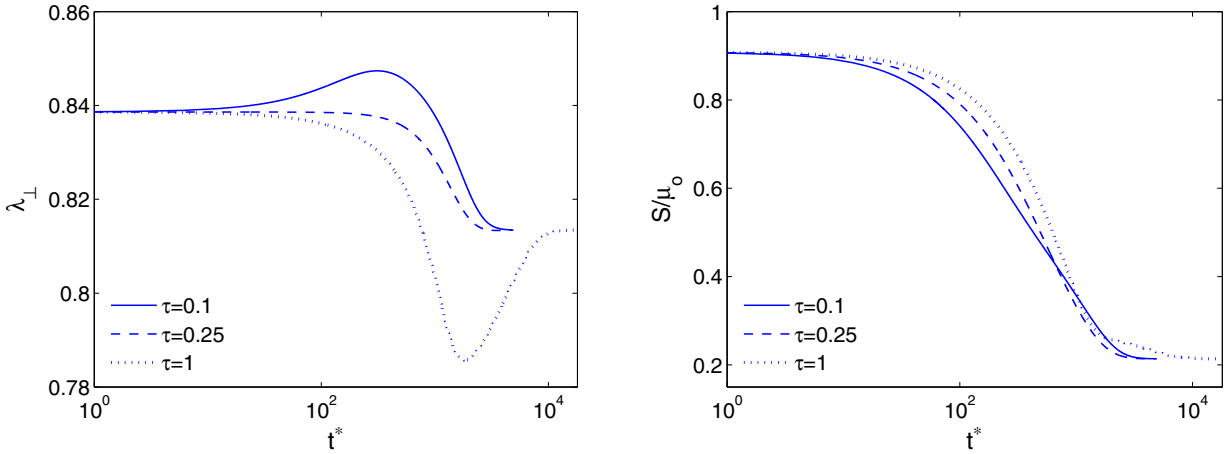

Figure 5. Transverse stretch $\lambda_\perp$ and nominal stress S/μ_o as a function of normalized time $t^* = t/t_m^*$ for material I with $\beta_f = 0.6$. Shown is the case of a hard loading device with $\lambda = 1.3$ and the degradation is of type MFF for all time. Here $n_f = n_m = 2$ and the non-dimensionalized time is defined by $t^* = t/t_m^*$. The three curves are for $\tau = 0.1$, 0.25, and 1.0.

increase in both α_m and α_f is governed by Equations (62) and (63). As $t \to \infty$ this gives $\alpha_m \to 1$, $\alpha_f \to 1$ and thus $\mu \to (1-\beta_m)\mu_0 = 0.2\mu_0$, $\gamma \to (1-\beta_f)\gamma_0 = 0.4\gamma_0$. Hence, as MFF degradation proceeds, the time evolution of the pair $(\lambda_\perp(t), \lambda)$ traces a horizontal path on the phase diagram that begins on the curve $\mathcal{C}_0$ and asymptotically approaches the point on the curve $\mathcal{C}_\infty^{MFF}$ corresponding to the given value of λ. Here, since $\mathcal{C}_\infty^{MFF}$ is to the left of $\mathcal{C}_0$ on the degradation phase diagram, the value of $\lambda_\perp$ must decrease; this is in contrast to the previously considered case of FF degradation where the value of $\lambda_\perp$ exhibited a monotonic increase in time. Figure 5 shows an example of this MFF degradation for $\lambda = 1.3$ using the three separate values: $\tau = 0.1$, 0.25, 1.0. In all three cases $S(t)$ is monotonically decreasing and so gives the anticipated stress relaxation as the material becomes increasingly damaged. However, $\lambda_\perp(t)$ is monotonically decreasing only for the case in which $\tau = 0.25$. The behavior of $\lambda_\perp$ is not monotone in the other two cases. In the case $\tau = 0.1$ the function $\lambda_\perp(t)$ is first increasing before exhibiting a monotonic decrease to its asymptotic value. For the case $\tau = 1$ the function $\lambda_\perp(t)$ is first decreasing to a value that is less than its asymptotic value before increasing to the asymptotic value. It is to be emphasized that the large time asymptotic value is the same in all three cases, namely $\lambda_\perp(\infty) = 0.8135$ as can be determined directly from the location on $\mathcal{C}_\infty^{MFF}$ where $\lambda = 1.3$. We now describe the affect that this has on the path traced out in the degradation phase diagram.

In the degradation phase diagram, the hard loading path with $\lambda = 1.3$ for the case $\tau = 0.25$ involves a leftward departure from $\mathcal{C}_0$ after which the path continues to the left as it approaches its asymptotic value on $\mathcal{C}_\infty^{MFF}$ as $t \to \infty$. Hence, for $\tau = 0.25$ the path is exactly the horizontal line segment from $\mathcal{C}_0$ to $\mathcal{C}_\infty^{MFF}$. In contrast, for the case $\tau = 0.1$ the path in the degradation phase diagram first involves a rightward departure from $\mathcal{C}_0$ before doubling back and approaching $\mathcal{C}_\infty^{MFF}$ as $t \to \infty$. For the case $\tau = 1.0$ the path in the degradation phase diagram departs leftward from $\mathcal{C}_0$ and then overshoots $\mathcal{C}_\infty^{MFF}$ before doubling back and approaching $\mathcal{C}_\infty^{MFF}$ as $t \to \infty$. The two cases of non-monotone $\lambda_\perp(t)$ each generate a doubling back of the trace of the path $(\lambda_\perp(t), \lambda)$ in the phase diagram. As indicated above, the example of $\tau = 1$ gives rise to an *overshoot*. The example of $\tau = 0.1$ gives rise to an *anomalous start-up* meaning that $\lambda_\perp(t)$ at $t = 0^+$ is initially increasing, in contrast to the eventual decrease that is required for the path to asymptotically approach $\mathcal{C}_\infty^{MFF}$ for large times.

The fact that $\lambda_\perp(t)$ need not be monotone for MFF degradation is due to the fact that MFF degradation is dependent upon the two different time scales t_m^* and t_f^* . If the fiber degradation time scale is much faster than the matrix degradation time scale, then, at least initially, the degradation tends to make $\alpha_f \to 1$ while α_m remains close to zero. This corresponds to $\gamma \to (1-\beta_f)\gamma_0$ with $\mu = \mu_0$. On this basis, the value of $\lambda_\perp$ is 'pulled', at least early in the degradation process, to the value associated with the curve of load states that is obtained by setting $\mu = \mu_0$ and $\gamma = 0.4\gamma_0$ in Equation (56). In other words the degradation path is initially attracted to the curve $\mathcal{C}_\infty^{FF}$. The curve $\mathcal{C}_\infty^{FF}$ is to the right of $\mathcal{C}_0$ and this gives an initial rightward departure from

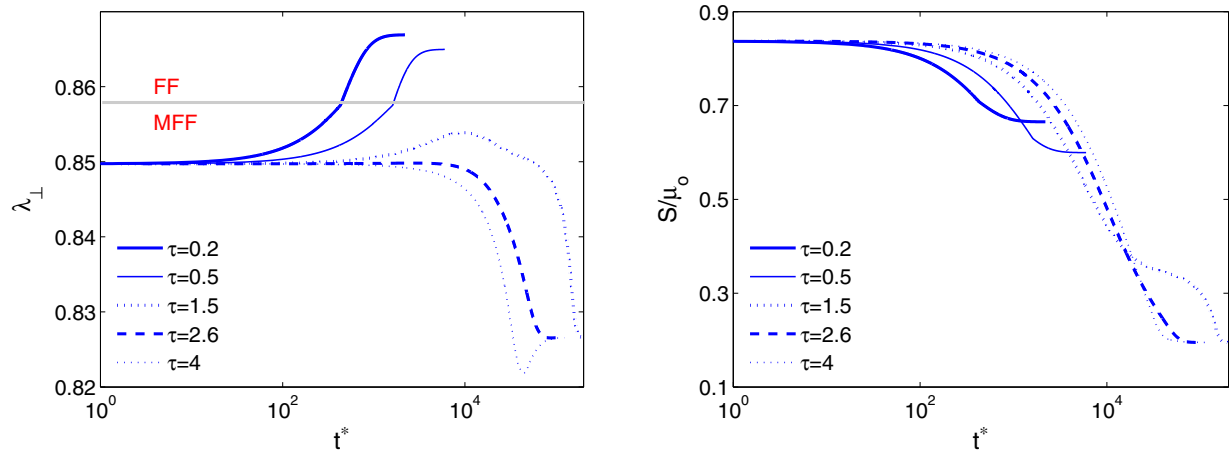

Figure 6. Transverse stretch $\lambda_\perp$ and nominal stress S/μ_o as a function of normalized time $t^* = t/t_m^*$ for material I with $\beta_f = 0.6$. Shown is the case of a hard loading device with $\lambda = 1.277$. Five responses are shown, each corresponding to a different value of τ. In the three cases of $\tau = 1.5$, 2.6, and 4 the degradation remains of type MFF or all time. In the two cases $\tau = 0.2$ and 0.5, the degradation is initially of type MFF region but then changes to type FF at some finite time into the hard loading process.

$\mathcal{C}_0$ as was observed for the above example when $\tau = 0.1$. Conversely, if the time scale for matrix degradation is much faster than that for fiber degradation, then, at least initially, the degradation tends to make $\alpha_m \to 1$ while α_f remains close to zero. This corresponds to $\mu \to (1 - \beta_m)\mu_0 = 0.2\mu_0$ and $\gamma \to \gamma_0$. On this basis, the value of $\lambda_\perp$ is 'pulled', at least early in the degradation process, to the value associated with the curve $\mathcal{C}_\infty^M$. The curve $\mathcal{C}_\infty^M$ is to the left of the curve $\mathcal{C}_\infty^{MFF}$ which is in turn to the left of the curve $\mathcal{C}_0$. In this case the path for $(\lambda_\perp(t), \lambda)$ overshoots its asymptotic state on $\mathcal{C}_\infty^{MFF}$ before doubling back to ultimately approach its asymptotic value on that curve. This was observed for the case $\tau = 1.0$ in Figure 5.

It therefore follows that if τ is relatively large, then the curve $\mathcal{C}_\infty^M$ can serve as an early time attractor for the path while it is in the MFF region of the degradation phase diagram. This caused the overshoot in Figure 5 for $\tau = 1.0$. Conversely, if τ is relatively small, then the curve $\mathcal{C}_\infty^{FF}$ can serve as an early time attractor for the path while it is in the MFF region of the degradation phase diagram. This caused the anomalous start-up in Figure 5 for $\tau = 0.1$. Since the initial value curve $\mathcal{C}_0$ is between these two curves it follows that $\mathcal{C}_\infty^M$ and $\mathcal{C}_\infty^{FF}$ form natural bounds for the path $(\lambda_\perp(t), \lambda)$ within the degradation phase diagram.

We now recall that the degradation is initially of type MFF if $\lambda > 1.275$ since $\mathcal{C}_0$ is within the MFF region for all such λ. On the basis of the above discussion it follows that the degradation will subsequently remain of type MFF for those values of λ which have the property that the line segment between $\mathcal{C}_\infty^M$ and $\mathcal{C}_\infty^{FF}$ is completely within the MFF region. A sufficiently close examination of Figure 3 would show that this property does not hold for all $\lambda > 1.275$ but does hold for $\lambda > 1.2785$. Here the value 1.2785 gives the particular value of λ where the curve $\mathcal{C}_\infty^{FF}$ intersects the boundary curve separating the MFF region from the FF region. For $\lambda > 1.2785$ the degradation will therefore remain of type MFF for all time, and the examples given in Figure 5 are representative of the various behaviors that can occur for that range of λ.

The final range of λ to consider for the hard device loading of material 1 with $\beta_f = 0.6$ is thus the small range of values $1.275 < \lambda < 1.2785$. In this case there are four basic qualitative behaviors for the function $\lambda_\perp(t)$. Three of these behaviors involve MFF degradation for all time while the fourth behavior involves MFF degradation which then abruptly changes to FF degradation. The three behaviors with MFF degradation for all time mirror the three basic behaviors that occur for $\lambda > 1.2785$ which were previously exhibited in Figure 5, namely: MFF behavior for all time with monotone decreasing $\lambda_\perp(t)$, MFF behavior for all time with $\lambda_\perp(t)$ that is first increasing and then decreasing, and MFF behavior for all time with $\lambda_\perp(t)$ that is first decreasing and then increasing. Consider an imposed stretch of $\lambda = 1.277$ which in turn makes $\lambda_\perp(0^+) = 0.850$. The three behaviors which have just been described are found to occur for the three values: $\tau = 2.6$, 1.5, and 4 (respectively) as shown in Figure 6.

Table 2. Hard device loading degradation behavior for material I with $\beta_f = 0.6$.

Stretch range	Degradation behavior
$1 < \lambda < 1.153$	No degradation
$1.153 < \lambda < 1.275$	FF degradation for all time, $\lambda_\perp$ monotone increasing
$1.275 < \lambda < 1.2785$	Initial MFF degradation that may or may not transition to FF degradation as determined by the degradation kinetics. This MFF degradation may involve monotone $\lambda_\perp$ or may instead involve either $\lambda_\perp$ overshoot (large τ) or $\lambda_\perp$ anomalous start-up (small τ). Transition to FF degradation requires $\lambda_\perp$ anomalous start-up with very small τ.
$\lambda > 1.2785$	MFF degradation for all time. This degradation may involve monotonic $\lambda_\perp$ or may instead involve either $\lambda_\perp$ overshoot (large τ) or $\lambda_\perp$ anomalous start-up (small τ).

The fourth type of qualitative behavior for the range of values $1.275 < \lambda < 1.2785$ is due to the fact that in this range of λ the curve $\mathcal{C}_\infty^{FF}$ is within the FF region. If the initial MFF degradation involves fiber degradation that is very much faster than matrix degradation it then follows that the value of $\lambda_\perp$ could be drawn into the FF degradation region. For $\lambda = 1.277$ the degradation phase diagram shows that this will occur if $\lambda_\perp$ exceeds the value 0.858. This behavior is shown in Figure 6 for both $\tau = 0.2$ and $\tau = 0.5$. In both of these cases the MFF degradation response causes $\lambda_\perp(t)$ to increase in a manner that is sufficient to cause $\lambda_\perp$ to hit the value 0.858 at some finite time. At that time the degradation shifts from type MFF to type FF.[6] There is then no further change in μ but the FF degradation makes for a continued decrease in γ. Subsequently, this causes $\lambda_\perp$ to increase monotonically, whereupon the path in the degradation phase diagram is drawn further to the right and hence further into the FF degradation region. As $t \to \infty$ it will again be the case that $\gamma \to (1 - \beta_f)\gamma_0 = 0.4\gamma_0$ while μ remains at whatever value it had when MFF degradation ceased. This value of μ will therefore be between μ_0 and $(1 - \beta_m)\mu_0 = 0.2\mu_0$. Because this final value of μ is less than μ_0 it follows that the asymptotic value of $\lambda_\perp$ will be less than that associated with the curve $\mathcal{C}_\infty^{FF}$. In other words the asymptotic location $(\lambda_\perp(\infty), 1.277)$ will be in the FF region but to the left of the curve $\mathcal{C}_\infty^{FF}$. The two separate values $\tau = 0.2$ and $\tau = 0.5$ illustrate how the asymptotic value $\lambda_\perp(\infty)$ is now dependent on the value of τ. While we have shown how the behavior $\lambda_\perp(t)$ exhibits a variety of different qualitative behaviors for λ obeying $1.275 < \lambda < 1.2785$, the behavior of $S(t)$ in all cases involves a monotonic decrease in time for the simple reason that, in all cases, the moduli μ and γ decrease with time (Figure 6).

Table 2 summarizes the different qualitative degradation behaviors described above for material 1 with $\beta_f = 0.6$ subject to a hard device tensile loading.

5.2. Material I with $\beta_f = 0.9$

Having just concluded a rather thorough discussion of hard loading for material 1 with $\beta_f = 0.6$ we now turn to consider hard loading for material 1 with $\beta_f = 0.9$. The degradation phase diagram in this case for $\lambda > 1$ is shown in Figure 7. Comparing this diagram with that for material 1 with $\beta_f = 0.6$ in Figure 3 it is seen that the only qualitative difference is that the curve $\mathcal{C}_0$ is now to the left of $\mathcal{C}_\infty^{MFF}$. This is due to the fact that now $\beta_f > \beta_m$. In addition there are small quantitative changes to the locations of the various curves and boundaries, and hence small changes in the locations of various curve intersections. For example, it is now the case that the curve $\mathcal{C}_0$ transitions from the N region to the FF region at $\lambda = 1.130$ and transitions from the FF region to the MFF region at $\lambda = 1.275$. The three locations where the FF–MFF boundary intersects with the curves $\mathcal{C}_0$, $\mathcal{C}_\infty^{MFF}$, and $\mathcal{C}_\infty^{FF}$ are of special significance in the following discussion. These intersections are given in Table 3.

There are now five separate intervals in which the hard device process for $\lambda > 1$ exhibits qualitatively different behavior, namely $1 < \lambda < 1.130$, $1.130 < \lambda < 1.2755$, $1.2755 < \lambda < 1.2781$, $1.2781 < \lambda < 1.2793$,

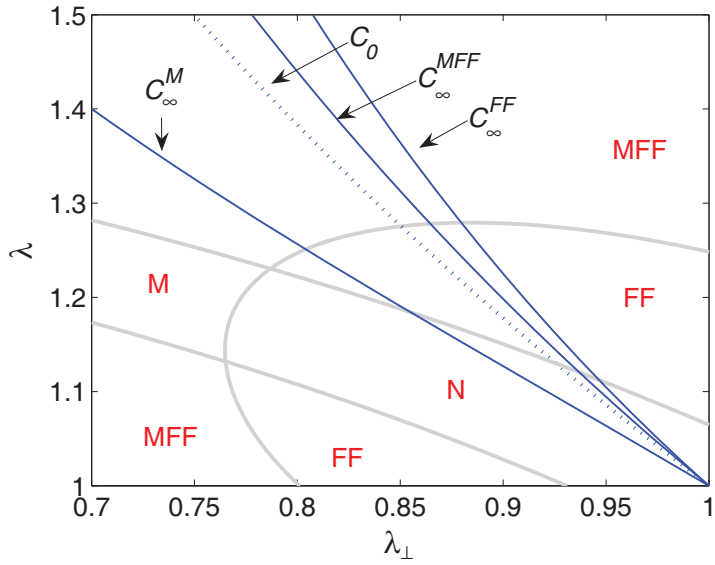

Figure 7. Degradation phase diagram for material 1 with $\beta_f = 0.9$ showing stretch state curves $\mathcal{C}_0$, $\mathcal{C}_\infty^M$, $\mathcal{C}_\infty^{FF}$, and $\mathcal{C}_\infty^{MFF}$.

Table 3. Intersection of the FF–MFF boundary with $\mathcal{C}_0$, $\mathcal{C}_\infty^{MFF}$, and $\mathcal{C}_\infty^{FF}$.

	$\mathcal{C}_0$	$\mathcal{C}_\infty^{MFF}$	$\mathcal{C}_\infty^{FF}$
FF–MFF boundary	$\lambda = 1.2755$	$\lambda = 1.2781$	$\lambda = 1.2793$

Table 4. Degradation behavior for material 1 with $\beta_f = 0.9$.

Stretch range	Degradation behavior for material 1 with $\beta_f = 0.9$
$1 < \lambda < 1.130$	No degradation
$1.130 < \lambda < 1.2755$	FF degradation for all time
$1.2755 < \lambda < 1.2781$	Initial MFF degradation that transitions to FF degradation
$1.2781 < \lambda < 1.2793$	Initial MFF degradation that may or may not transition to FF degradation as determined by the degradation kinetics
$\lambda > 1.2793$	MFF degradation for all time

and $\lambda > 1.2793$. The basic aspects of this behavior can be extracted from a thoughtful consideration of the degradation phase diagram in Figure 7. Table 4 summarizes this qualitative behavior.

We now elaborate on the claims presented in Table 4. To begin with, we omit until a later paragraph any consideration of the stretch range $1.2755 < \lambda < 1.2781$. This is because each of the other four stretch ranges have an associated degradation behavior that corresponds to one of the four behaviors present in material 1 for the previously considered value $\beta_f = 0.6$ (summarized in Table 2).

The reason for the four behaviors on $1 < \lambda < 1.130$, $1.130 < \lambda < 1.2755$, $1.2781 < \lambda < 1.2793$, and $\lambda > 1.2793$ follows on the basis of the same type of considerations as was the case for material 1 with $\beta_f = 0.6$. Namely, in the FF region the path traced out by $(\lambda_\perp(t), \lambda)$ moves to the right as γ decreases and asymptotically approaches $\mathcal{C}_\infty^{FF}$ if there is no matrix degradation whatsoever. Similarly, in the MFF region the response is restricted to be within the curves $\mathcal{C}_\infty^M$ and $\mathcal{C}_\infty^{FF}$. If the matrix degradation operates on a sufficiently faster time scale than that of the fiber degradation, then $\mathcal{C}_\infty^M$ may serve as a short time attractor for the path $(\lambda_\perp(t), \lambda)$. Alternatively, $\mathcal{C}_\infty^{FF}$ may serve as a short time attractor for the path in the MFF region in the event that

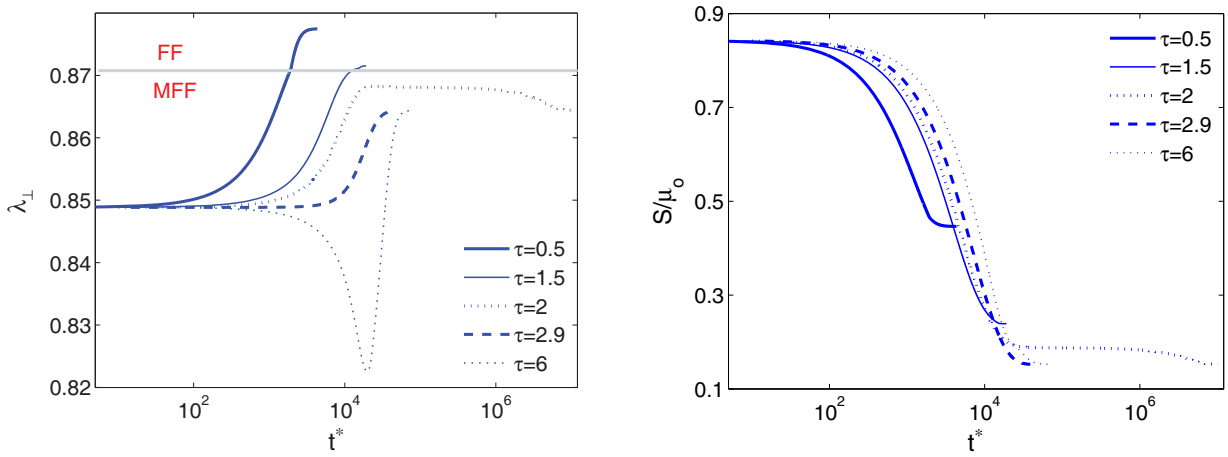

Figure 8. Evolution of $\lambda_\perp$ and S/μ_o with t^* for a hard loading device for material I with $\beta_f = 0.9$ and $\lambda = 1.2788$. Other parameters: $\beta_m = 0.8$, and $n_f = n_m = 2$.

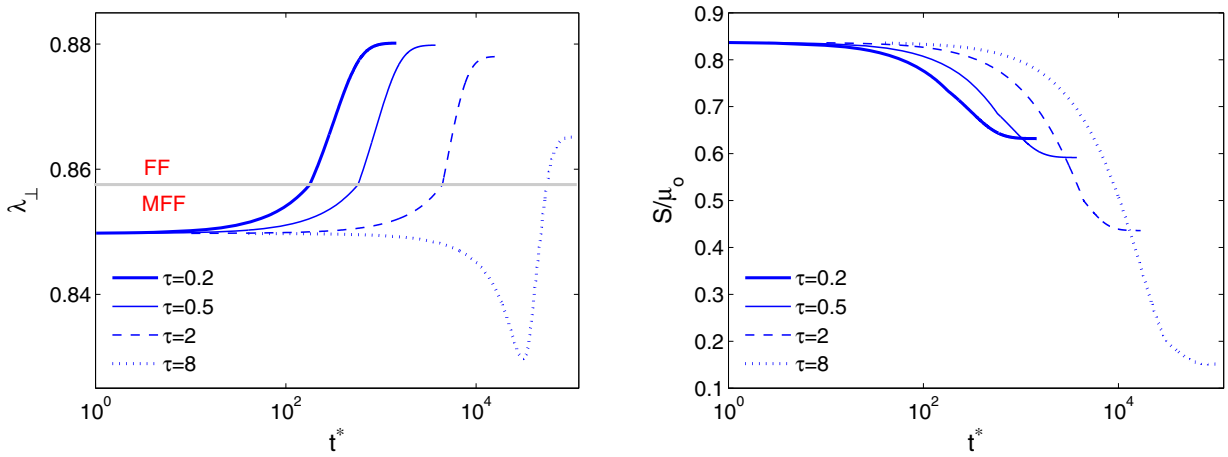

Figure 9. Evolution of $\lambda_\perp$ and S/μ_o with t^* for a hard loading device for material I with $\lambda = 1.277$ and $\beta_f = 0.9$. Other parameters: $\beta_m = 0.8$ and $n_f = n_m = 2$. Four values of τ are used, three of which give a monotone $\lambda_\perp(t)$ and one of which gives an anomalous start-up.

the fiber degradation is much faster than the matrix degradation. Paths that remain in the MFF region approach the corresponding point on $\mathcal{C}_\infty^{MFF}$ as $t \to \infty$.

For example, we recall for material 1 with $\beta_f = 0.6$ that the range $1.275 < \lambda < 1.2785$ corresponds to an initial MFF degradation that may or may not transition to FF degradation as determined by the degradation kinetics (as shown in Figure 6). For material 1 with $\beta_f = 0.9$ the corresponding range for such behavior is $1.2781 < \lambda < 1.2793$. An example of λ in this range is the value $\lambda = 1.2788$ as illustrated in Figure 8. This figure shows $\lambda_\perp(t)$ and $S(t)$ for five values of τ, three of which give MFF for all time and two of which give a transition to FF. The three values of τ that illustrate MFF degradation for all time show the three different qualitative behaviors for $\lambda_\perp(t)$ that were also shown in Figure 6: monotone, overshoot, and anomalous start-up. The conspicuous difference is that now MFF degradation for all time gives $\lambda_\perp(\infty) > \lambda_\perp(0^+)$ so that, for example, the monotone behavior of $\lambda_\perp(t)$ now involves monotone increase instead of monotone decrease. This is due to the fact that $\mathcal{C}_0$ is to left of $\mathcal{C}_\infty^{MFF}$ when $\beta_f = 0.9$, which is opposite to the ordering of these two curves for $\beta_f = 0.6$. This in turn alters how large or small τ correspond to either overshoot or anomalous start-up for MFF degradation. For example the overshoot possibility, which now involves increase of $\lambda_\perp(t)$ followed by

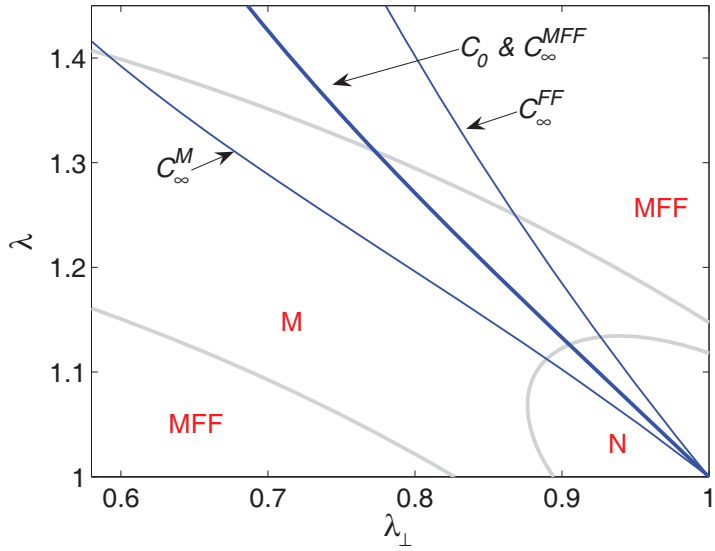

Figure 10. Degradation phase diagram for material 2 showing stretch state curves $\mathcal{C}_0$, $\mathcal{C}_\infty^M$, and $\mathcal{C}_\infty^{FF}$. For this material, since $\beta_f = \beta_m$ the curves $\mathcal{C}_0$ and $\mathcal{C}_\infty^{MFF}$ are coincident.

decrease, is generated by a relatively fast fiber degradation, which is opposite to the MFF time scale ordering that gives overshoot when $\beta_f = 0.6$.

Finally, for material 1 with $\beta_f = 0.9$ we consider the stretch range $1.2755 < \lambda < 1.2781$ which gives a degradation behavior unlike any that occurs for material 1 with $\beta_f = 0.6$. In this stretch range the original MFF type degradation is guaranteed to terminate at finite time after which the degradation is guaranteed to be of type FF. This is again because of the ordering of the various curves. Namely, for this stretch range the curve $\mathcal{C}_0$ is in the MFF degradation region, but the curve $\mathcal{C}_\infty^{MFF}$ is in the FF degradation region. Thus, as $\mathcal{C}_\infty^{MFF}$ attracts the value $\lambda_\perp(t)$ for large time during the MFF degradation it is inevitable that $(\lambda_\perp(t), \lambda)$ will be drawn into the FF degradation region. Once drawn into this region, the ensuing FF degradation pulls the path point further to the right, although not as far as $\mathcal{C}_\infty^{FF}$ because $\mu < \mu_0$ due to the matrix degradation during the MFF degradation phase. Thus, once the path is captured by the FF degradation region it remains trapped within this region for all subsequent time. This is illustrated in Figure 9 for $\lambda = 1.277$. As shown in this figure, the behavior of $\lambda_\perp$ may be monotone or may exhibit anomalous start-up. However, now the overshoot-type behavior does not occur because, after the transition to FF degradation, there is then only one time scale governing the fiber degradation in the present modeling.

5.3. Material 1 with $\beta_f = 1$

We conclude the discussion of hard loading for material 1 with a brief comment regarding the case in which $\beta_f = 1$. In this case the degradation phase diagram and the ordering of the curves remain qualitatively the same as that for material 1 with $\beta_f = 0.9$. In particular the curves are ordered: $\mathcal{C}_\infty^M$, $\mathcal{C}_0$, $\mathcal{C}_\infty^{MFF}$, $\mathcal{C}_\infty^{FF}$ as one proceeds from left to right for $\lambda > 1$. It follows that the degradation behavior mirrors that of material 1 with $\beta_f = 0.9$. The main quantitative difference is that there are small changes in the stretch values λ that demarcate the five different behavior range possibilities which were indicated previously in Table 4. Here we note, and this is the reason why we here briefly consider material 1 with $\beta_f = 1$, that the equation for $\mathcal{C}_\infty^{FF}$ is simply $\lambda_\perp = \lambda^{-1/2}$ when $\beta_f = 1$. Thus, the large time behavior for this material under FF degradation approaches that of the isotropic matrix material. This is true both for the case where the degradation is always of FF type and for the case where the material transitions to FF degradation after an initial period of MFF degradation. In other words, if $\beta_f = 1$, then FF degradation that continues unabated for all time asymptotically eradicates the fibrous component. This results in a formally isotropic material in the limit $t \to \infty$.

Table 5. Hard device degradation behavior for material 2.

Stretch range	Degradation behavior
$1 < \lambda < 1.126$	No degradation
$1.126 < \lambda < 1.311$	M degradation for all time, $\lambda_\perp$ monotone decreasing
$1.311 < \lambda < 1.402$	Initial MFF degradation that may or may not transition to M degradation as determined by the degradation kinetics. The MFF degradation may involve either $\lambda_\perp$ departing leftward (large τ) or rightward (small τ). Transition to M degradation requires $\lambda_\perp$ leftward start-up (very large τ).
$\lambda > 1.402$	MFF degradation for all time, this degradation may involve either $\lambda_\perp$ departing to the left (large τ) or to the right (small τ).

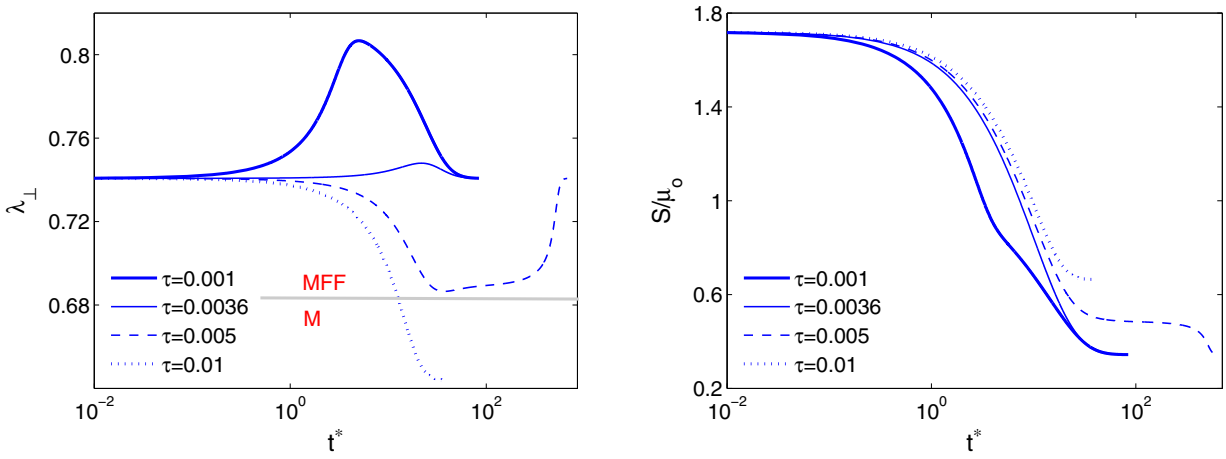

Figure 11. Evolution of $\lambda_\perp$ and S/μ_o with t^* for a hard loading device with material 2 and $\lambda = 1.36$. For this value of λ the degradation is initially of type MFF but may transition to type M depending on the kinetics. Four values of τ are shown, one of which gives a transition to M degradation and three of which do not.

5.4. Material 2

We now consider the hard device loading for material 2. The curves $\mathcal{C}_0$ and $\mathcal{C}_\infty^{MFF}$ are coincident for this material since $\beta_f = \beta_m$. We also recall from Figure 2 that there is no FF degradation region in this case. Figure 10 shows the degradation phase diagram for this material along with the stretch state curves. The curve $\mathcal{C}_0$ intersects the N–M boundary at $\lambda = 1.126$ and intersects the M–MFF boundary at $\lambda = 1.311$. The only other intersection of qualitative significance is that which occurs between the curve $\mathcal{C}_\infty^M$ and the M–MFF boundary. This intersection occurs at $\lambda = 1.402$.

The qualitative degradation behavior for material 2 subject to hard device tensile loading can now be extracted from Figure 10 on the basis of the previous logical considerations. As indicated in Table 5 there are four separate ranges of λ that involve different qualitative behavior.

The degradation is guaranteed to be of type MFF for all time if $\lambda > 1.402$. In addition, if $1.311 < \lambda < 1.402$, then the degradation is initially of type MFF and will remain of type MFF if τ is sufficiently small. Degradation that remains of type MFF for all time involves a transverse stretch such that $\lambda_\perp(\infty) = \lambda_\perp(0^+)$ by virtue of the coincidence of $\mathcal{C}_0$ and $\mathcal{C}_\infty^{MFF}$. Thus, when the degradation is of type MFF for all time then any departure of $\lambda_\perp(t)$ from its initial value may formally be viewed as an anomalous start-up. In this case the two time scales t_m^* and t_f^* affect $\lambda_\perp(t)$; the faster of the two time scales then dominates the $\lambda_\perp$ start-up kinetics and the slower time scale dominates the $\lambda_\perp$ return kinetics. The stress is once again monotonically decreasing. Figure 11 shows example behavior for $\lambda = 1.36$.

Table 6. Soft device degradation behavior for material I with $\beta_f = 0.9$.

Stress range	Soft device degradation behavior
$0 < S/\mu_0 < 0.395$	No degradation
$0.395 < S/\mu_0 < 0.688$	FF degradation for all time
$0.688 < S/\mu_0 < 0.832$	Initial FF degradation that transitions to MFF degradation
$S/\mu_0 > 0.832$	MFF degradation for all time

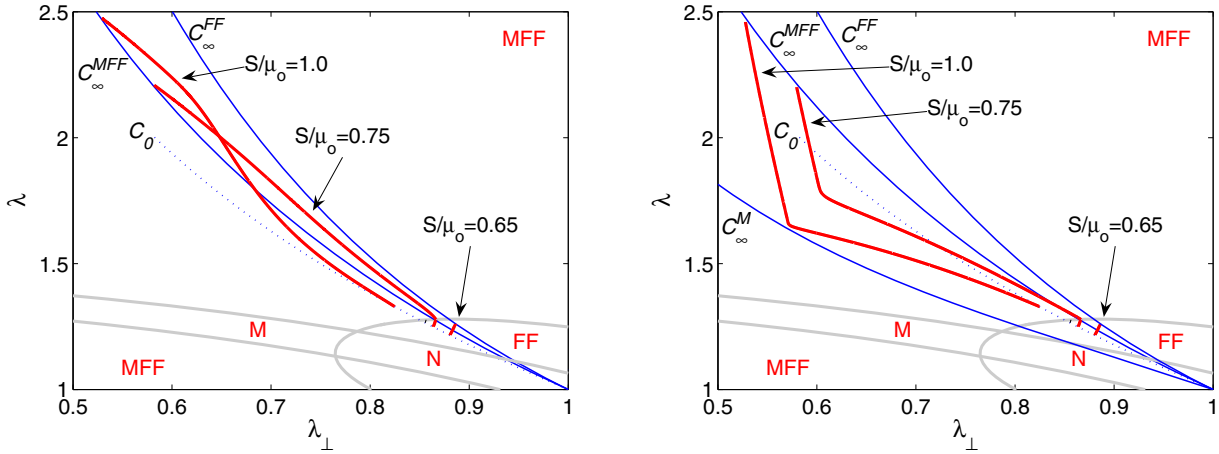

Figure 12. Degradation paths $(\lambda_\perp(t), \lambda(t))$ for soft loading of material I with $\beta_f = 0.9$ for $\tau = 0.1$ (left) and $\tau = 5$ (right).

6. Soft loading device

6.1. Material I with $\beta_f = 0.9$

For material 1 with $\beta_f = 0.9$ we recall that the hard loading device gave five separate qualitatively different degradation ranges for λ as described in Table 4. For soft device tensile loading of this same material there are four separate qualitatively different degradation ranges for S as described in Table 6.

A conspicuous difference between the hard and soft device tensile loading of this material is that in hard device loading there is MFF degradation that transitions to FF degradation, but not vice versa, whereas in soft device loading there is FF degradation that transitions to MFF degradation, but not vice versa. We now indicate how we arrive at these conclusions and discuss the associated behaviors in more detail.

The upper bound value $S = 0.395\mu_0$ for the range of S that gives no degradation follows from Equation (57) and (58) using the location $(\lambda_\perp, \lambda) = (0.926, 1.130)$ where $\mathcal{C}_0$ intersects the N–FF boundary. The range of S that gives no degradation in soft loading exactly corresponds to the range of λ that gives no degradation in hard loading. For the other degradation scenarios there is no longer any such simple correspondence between the soft and hard loading device behaviors.

For S in the next range, $0.395\mu_0 < S < 0.688\mu_0$, the degradation is initially of type FF and the degradation path $(\lambda_\perp(t), \lambda(t))$ remains within the FF region while being attracted to an appropriate point on the curve $\mathcal{C}_\infty^{FF}$. As an example, the degradation path for $S = 0.65\mu$ is shown in Figure 12. Such a path is completely determined from Equations (56), (57), and (58) by holding S and μ_0 fixed and letting γ decrease from its initial value γ_0 to its final value $(1-\beta_f)\gamma_0 = 0.1\gamma_0$. The largest value of S that keeps such a path within the FF degradation region is determined from Equations (57) and (58) using the location $(\lambda_\perp, \lambda) = (0.880, 1.279)$ where $\mathcal{C}_\infty^{FF}$ intersects the FF–MFF boundary. On this basis one obtains the upper bound value $S = 0.688\mu_0$ in Table 6 for the range of S that gives FF degradation for all time.

For S in the next range, $0.688\mu_0 < S < 0.832\mu_0$, the degradation is initially of type FF but the degradation path encounters the FF–MFF boundary as it is attracted to $\mathcal{C}_\infty^{FF}$. The upper bounding value $S = 0.832\mu_0$ for

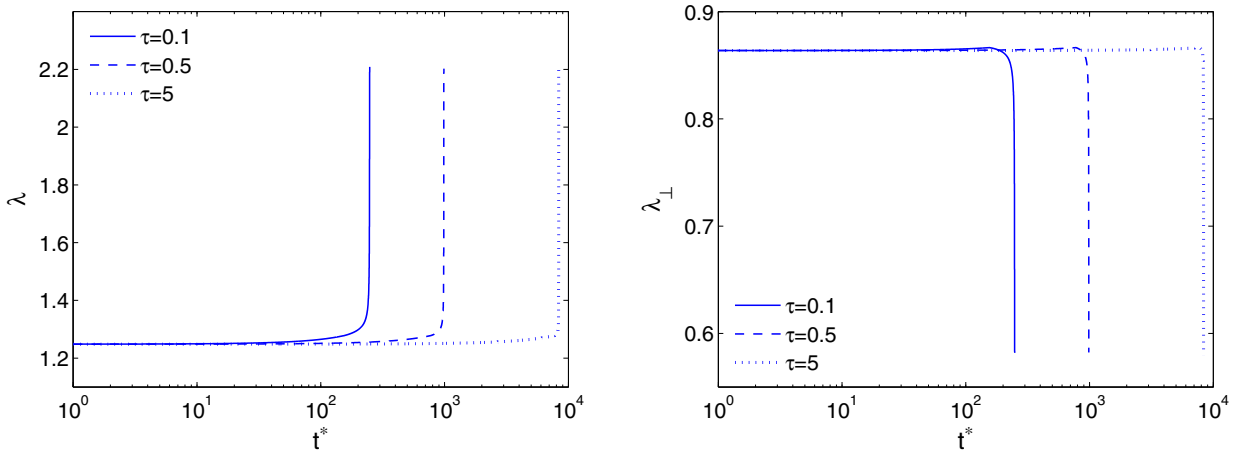

Figure 13. Axial stretch λ and transverse stretch $\lambda_\perp$ as a function of normalized time $t^* = t/t_m^*$ for material I with $\beta_f = 0.9$ at the fixed value $S = 0.75\mu_0$. For this value of S the degradation is initially of type FF but then changes into type MFF. The creep-type response for three different values of τ are shown, $\tau = 0.1$, 0.5, and 5.

this behavior follows from the location $(\lambda_\perp, \lambda) = (0.850, 1.275)$ where $\mathcal{C}_0$ intersects the FF–MFF boundary. For these values of S the initial portion of the degradation path $(\lambda_\perp(t), \lambda(t))$ is in the FF region, and this initial portion can again be obtained directly from Equations (56), (57), and (58). However after the degradation path enters the MFF region it can no longer be determined solely from those equations since the degradation kinetics determines how the ratio γ/μ changes with time. This is why Figure 12 consists of two separate panels, the left panel is for $\tau = 0.1$ and the right panel is for $\tau = 5$. For the previous ranges of S under consideration, i.e. $S < 0.688\mu_0$, the degradation path was unaffected by τ which is why the short path for $S = 0.65\mu_0$ is the same in both panels. However, for $S > 0.688\mu_0$ the degradation path is highly dependent upon τ in the MFF degradation region. The paths for $S = 0.75\mu_0$ are shown in the two panels of Figure 12. The two paths are identical so long as the path is within the FF degradation region. However, once the path enters the MFF degradation region the effect of τ is apparent from the figure. In particular, the path for $\tau = 0.1$ remains above the curve $\mathcal{C}_\infty^{MFF}$ while the path for $\tau = 5$ does not. In both cases the path is confined to that portion of the MFF degradation region that is between $\mathcal{C}_\infty^{M}$ and $\mathcal{C}_\infty^{FF}$. Also, in both cases, as $t \to \infty$ the path approaches a common location on $(\lambda_\perp(\infty), \lambda(\infty))$ on $\mathcal{C}_\infty^{MFF}$. This asymptotic value can be determined exactly on the basis of Equations (56), (57), and (58) for the given value of S by taking $\mu = (1 - \beta_m)\mu_0 = 0.4\mu_0$ and $\gamma = (1 - \beta_f)\gamma_0 = 0.1\gamma_0$.

Graphs showing the time-dependent functions $\lambda(t)$ and $\lambda_\perp(t)$ with $S = 0.75\mu_0$ for three different τ are shown in Figure 13. In particular, the graph of $\lambda(t)$ exhibits the anticipated creep-type elongation as the material weakens. More generally all of the degradation paths in Figure 12 show λ increasing along the degradation path; hence, the creep-type elongation is a general feature of tensile soft loading when degradation takes place. In contrast, $\lambda_\perp$ in Figure 13 is slightly non-monotone since $\lambda_\perp$ increases during the FF degradation portion of the path, but decreases during the MFF degradation portion of the path (see again Figure 12).

Similar considerations govern the remaining range $S > 0.832\mu_0$ where the degradation is of type MFF for all time. Once again the degradation path connects the initial point $(\lambda_\perp(0^+), \lambda(0^+))$ on $\mathcal{C}_0$ to the asymptotic point $(\lambda_\perp(\infty), \lambda(\infty))$ on $\mathcal{C}_\infty^{MFF}$, both of which can be determined *a priori* without consideration of the path kinetics. However, for $0 < t < \infty$ the determination of $(\lambda_\perp(t), \lambda(t))$ requires the consideration of the kinetic equations (62) and (63). In particular, for large τ the degradation path will swing towards $\mathcal{C}_\infty^{M}$, with a relatively closer approach for larger τ. In a similar fashion the degradation path will swing towards $\mathcal{C}_\infty^{FF}$ for relatively small τ. Specifically, the effect of τ on the path trajectory for this range of S is shown in Figure 12 for $S = \mu_0$.

6.2. Material 2

As a final example we consider the soft device loading for material 2. There are then four basic degradation behaviors as described in Table 7. We recall for this material that $\beta_m = \beta_f$ gives $\mathcal{C}_0 = \mathcal{C}_\infty^{MFF}$.

Table 7. Soft device degradation behavior for material 2.

Stress range	Degradation behavior
$0 < S/\mu_0 < 0.47$	No degradation
$0.47 < S/\mu_0 < 0.96$	M degradation for all time
$0.96 < S/\mu_0 < 1.40$	Initial M degradation that transitions to MFF degradation
$S/\mu_0 > 1.40$	MFF degradation for all time

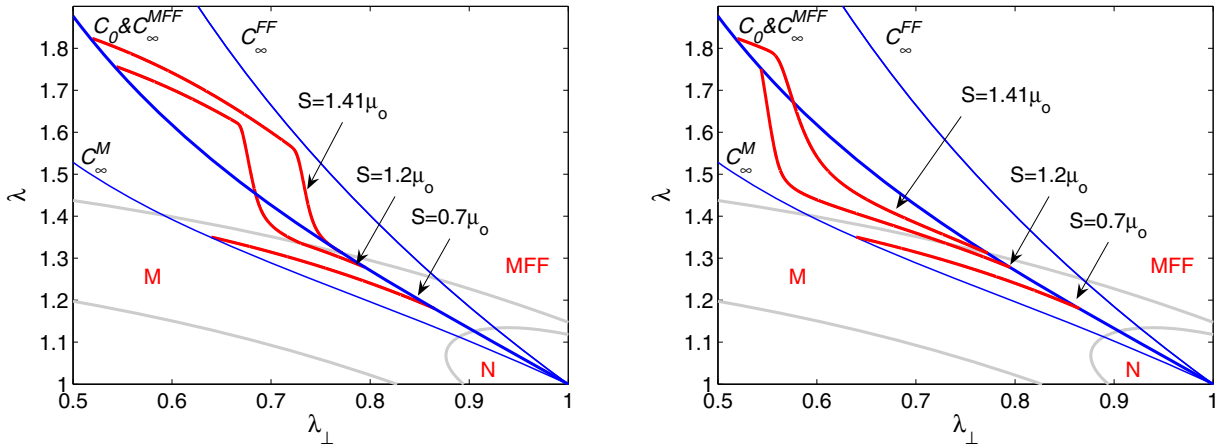

Figure 14. Degradation paths $(\lambda_\perp(t), \lambda(t))$ for soft loading of material 2 for $\tau = 0.001$ (left) and $\tau = 0.01$ (right).

Similar to the case of material 1, in soft device loading there is the possibility of initial M degradation that transitions to MFF degradation, but not vice versa, whereas in hard device loading for this material there is the possibility of MFF degradation that transitions to M degradation, but not vice versa. The value $S = 0.47\mu_0$ that demarcates the upper bound for no degradation is found by first locating the point $(\lambda_\perp, \lambda) = (0.905, 1.126)$ where the curve $\mathcal{C}_0$ intersects the N–M boundary and then calculating S from Equations (57) and (58) using $\mu = \mu_0$ and $\gamma = \gamma_0$. It follows that the range of S for no degradation under soft loading corresponds exactly to the range of λ for no degradation under hard loading.

The next range, $0.47\mu_0 < S < 0.96\mu_0$, gives M degradation for all time. In this range the degradation paths $(\lambda_\perp(t), \lambda(t))$ are completely determinable from Equations (56), (57), and (58) by holding S and γ_0 fixed and letting μ decrease from its initial value μ_0 to its final value $(1 - \beta_m)\mu_0 = 0.2\gamma_0$. In particular, $\lambda(t)$ is increasing and the large time asymptotic point $(\lambda_\perp(\infty), \lambda(\infty))$ is on the curve $\mathcal{C}_\infty^M$. The degradation path for $S = 0.7\mu_0$ that is determined in this fashion is shown in Figure 14. The upper bound value of S for this type of behavior, namely $S = 0.96\mu_0$, may be found by first locating the point $(\lambda_\perp, \lambda) = (0.591, 1.402)$ where the curve $\mathcal{C}_\infty^M$ intersects the M–MFF boundary, and then using these values to calculate S from Equations (57) and (58) upon taking $\gamma = \gamma_0$ and $\mu = (1 - \beta_m)\mu_0 = 0.2\mu_0$.

The range $0.96\mu_0 < S < 1.40\mu_0$ gives an initial M degradation that then changes to MFF degradation because the degradation path crosses the M–MFF boundary. The path does not depend upon τ while undergoing M degradation, but as soon as the path enters the MFF degradation region then the effect of τ becomes pronounced. This again accounts for the two panel depiction in Figure 14. As in the example of material 1 with soft loading, relatively large values of τ cause the path to swing toward $\mathcal{C}_\infty^M$ and relatively small values of τ cause the path to swing toward $\mathcal{C}_\infty^{FF}$. This is shown in Figure 14 for $S = 1.2\mu_0$. Once again the $t \to \infty$ point $(\lambda_\perp(\infty), \lambda(\infty))$ is independent of τ and can be located on the curve $\mathcal{C}_\infty^{MFF}$. The upper bound value $S = 1.40\mu_0$ for this range of behavior is found by first locating the point $(\lambda_\perp, \lambda) = (0.773, 1.311)$ where the curve $\mathcal{C}_0$ intersects the M–MFF boundary and then these values are used to calculate S from Equations (57) and (58) upon taking $\mu = \mu_0$ and $\gamma = \gamma_0$.

Finally for $S > 1.40\mu_0$ the degradation is of type MFF for all time so that the full path is dependent upon the kinetic parameter τ as illustrated in Figure 14 for $S = 1.41\mu_0$. Once again the asymptotic value $(\lambda_\perp(\infty), \lambda(\infty))$ is independent of τ and can be located on the curve $\mathcal{C}_\infty^{MFF}$. In particular, the initial values of λ and $\lambda_\perp$ follow from Equations (56), (57), and (58) using $\gamma = \gamma_0$ and $\mu = \mu_0$ whereas the $t \to \infty$ asymptotic values follow from these same equations using $\gamma = 0.2\gamma_0$ and $\mu = 0.2\mu_0$. The degradation path between the initial and final points is again dependent upon the kinetics.

7. Summary and applications

By extending the framework of [3] to the case of multiple degradation variables one is able to model multi-component material systems wherein each component is subject to its own specific mechanism of damage accumulation. Here, we have considered the case of a material with two fiber families within a surrounding matrix, all of which are potentially subject to degradation. As in [3] the modeling is in terms of two constitutive functions, a Helmholtz stored energy density W and a rate of mechanical energy dissipation function $\hat{\xi}$. The energy W is a function of the damage variables (here α_m, α_{f_1}, and α_{f_2}) and of the usual strain invariants and pseudo-invariants describing the anisotropic symmetry class of interest (see [6]). Here we have used I_1, $I_4^{(1)}$, and $I_4^{(2)}$ as given in (19)–(21) for this purpose. More generally, one may let W depend upon $\mathrm{tr}\mathbf{C}^2$ and, since the material consists of two fiber families, the additional pseudo-invariants $\mathbf{M}^{(1)}\cdot\mathbf{C}^2\mathbf{M}^{(1)}$, $\mathbf{M}^{(2)}\cdot\mathbf{C}^2\mathbf{M}^{(2)}$, $\mathbf{M}^{(1)}\cdot\mathbf{C}\mathbf{M}^{(2)}$. Here we chose to concentrate early in the development on the specific model in Equation (18) which does not employ these additional quantities. In a similar fashion the rate of dissipation function $\hat{\xi}$ may also depend upon these damage variables, invariants and pseudo-invariants while also being dependent upon the time derivatives of the damage variables. Here again we focused on the specific form (32)–(34) which has no explicit dependence upon the finite strain.

Even in this specific and relatively simple context one obtains a mathematically rich description of the resulting material behavior. This was demonstrated here for a uniform material with equal-property fibers under a uniaxial loading that is symmetric with respect to the two fiber orientations. Then, in addition to the possibility that no degradation takes place, there are three non-trivial degradation possibilities: matrix degradation (M), fiber degradation (FF), and degradation of both the fibrous and matrix components (MFF). What is perhaps most striking is how even the simple loadings of suddenly applied constant stretch (hard loading) and suddenly applied constant force (soft loading) can lead to unexpected transition possibilities between the three non-trivial degradation scenarios. This was demonstrated in Sections 5 and 6 with the aid of special material parameter choices. For example, it was shown for one such material (material 1 with $\beta_f = 0.9$) that hard device loading can give an MFF degradation that eventually transitions to the simpler FF degradation. However, the hard device loading for this material cannot give the converse, namely an initial FF degradation that eventually transitions to an MFF degradation. It is therefore quite interesting that this same material has an opposite type behavior when subject to soft device loading. Namely, certain suddenly applied levels of force give an FF degradation that eventually transitions to an MFF degradation, however there are no values of force which, when suddenly applied, give an MFF degradation that eventually transitions to an FF degradation.

In order to demonstrate such behavior and to uncover the myriad of transition-dependent degradation possibilities for both the hard and soft device we have constructed degradation phase diagrams in a two-dimensional stretch space. Within this diagram we then plotted four additional curves: the curve of initial (suddenly loaded) states $\mathcal{C}_0$, the curve of asymptotic states for the M region $\mathcal{C}_\infty^M$, the curve of asymptotic states for the FF region $\mathcal{C}_\infty^{FF}$, and the curve of asymptotic states for the MFF region $\mathcal{C}_\infty^{MFF}$. By considering how these curves both attract and bound the stretch path we are able to provide significant insight as to the overall qualitative behavior of the system as it degrades. This is especially important for the case of MFF degradation which, unlike the simpler M and FF degradation, has a dependence on the separate time scales for matrix and fiber degradation. This causes the degradation path in the MFF region to display a wide range of qualitative behaviors. As shown here, these behaviors are systematically revealed by an analysis that combines asymptotic and computational analysis.

One aim of such modeling is to characterize biodegradable polymers which are currently experiencing significant development with applications to tissue engineering [24, 25], medical implantable devices [26, 27], and drug delivery [28, 29]. In particular, tissue engineering applications require biodegradable scaffolds

with mechanical properties (e.g. porosity, anisotropy) similar to that of the original tissue. Recent advances in electrospinning technology make electrospun fiber-reinforced composites an excellent candidate for such applications in a variety of different tissues including vascular, bone, and tendon [30, 25, 31]. Such biodegradable scaffolds must provide mechanical support *in vivo* while the tissue heals with the possible additional requirement that any scaffold remnant is removable when the healing process is complete. Fine control of the rate of the degradation, so as to precisely couple with the change of mechanical properties of the healing tissue, is a central aim of such medical interventions. The type of modeling presented here, when formulated in the context of an appropriate boundary value problem that describes the scaffold geometry, may provide a theoretical foundation for quantitative characterization of specific fiber–matrix composite constructs.

Notes

1. The study [8] makes use of a description for swelling that takes volumetric expansion as a prescribed quantity and the reader is referred to [8] as well as the numerous other sources (e.g. [9, 10, 11, 12, 13]) that provide extended discussion on the many ways in which swelling can be described in large-deformation continuum mechanics.
2. Equation $(1)_2$ corrects the typo in equation $(3)_2$ of [8] which inadvertently included a transpose.
3. The possibility of symmetry-breaking bifurcation is not considered here.
4. Note from (29) that Λ_m has units of [stress][time]$^{1/n_m}$. It is convenient to define Λ_m in this fashion because it permitted a simple expression within (35).
5. Here and in what follows the use of the terminology *full fiber degradation* is short for the fully allowed fiber degradation as determined by the constitutive parameter β_f. A corresponding meaning will be attached to the terminology *full matrix degradation*.
6. The time at which the transition from MFF to FF occurs is dependent upon τ and so is different for the two cases $\tau = 0.2$ and $\tau = 0.5$.

Funding

This research received no specific grant from any funding agency in the public, commercial, or not-for-profit sectors.

Conflict of Interest

None declared.

References

[1] Chen, R, Yoon, M, Smalley, A, Johnson, DC, and Tyler, DR. Investigation of the origin of tensile stress-induced rate of enhancements in the photochemical degradation of polymer. *Journal of American Chemical Society* 2004; 126: 3054–3055.
[2] Smit, TH, Engels, TAP, Söntjens, SHM, and Govaert, LE. Time-dependent failure in load-bearing polymers: a potential hazard in structural applications of polylactides. *Journal of Material Science: Materials in Medicine*, 2010; 21: 871–878.
[3] Rajagopal, KR, Srinivasa, AR, and Wineman, AS. On the shear and bending of a degrading polymer beam. *International Journal of Plasticity* 2007; 23: 1618–1636.
[4] Ziegler, H, and Wehrli, C. The derivation of constitutive equations from the free energy and the dissipation function. *Advances in Applied Mechanics* 2006; 25: 183–238.
[5] Ogden, RW. *Non-linear Elastic Deformations*. Chichester: Ellis Horwood, 1984.
[6] Holzapfel, GA. *Nonlinear Solid Mechanics: A Continuum Approach for Engineering*. Chichester: Wiley, 2000.
[7] Soares, JS, Rajagopal, KR, and Moore, JE Jr. Deformation-induced hydrolysis of a degradable polymeric cylindrical annulus. *Biomechanics and Modeling in Mechanobiology* 2010; 9: 177–186.
[8] Baek, S, and Pence, TJ. On swelling induced degradation of fiber reinforced polymers. *International Journal of Engineering Science* 2009; 47: 1100–1109.
[9] Treloar, LRG. *The Physics of Rubber Elasticity*. Oxford: Oxford University Press, 1975.
[10] Rajagopal, KR, and Tao, L. *Mechanics of Mixtures*. Singapore: World Scientific, 1996.
[11] Baek, S, and Srinivasa, AR. Diffusion of a fluid through an elastic solid. *International Journal of Nonlinear Mechanics* 2004; 39: 201–218.
[12] Tsai, H, Pence, TJ, and Kirkinis, E. Swelling induced finite strain flexure in a rectangular block of an isotropic elastic material. *Journal of Elasticity* 2004; 79: 68–89.
[13] Deng, H, and Pence, TJ. Equilibrium states of mechanically loaded saturated and unsaturated polymer gels. *Journal of Elasticity* 2010; 99: 39–73.

[14] Merodio, J, and Ogden, RW. Mechanical response of fiber-reinforced incompressible nonlinearly elastic solids. *International Journal of Nonlinear Mechanics* 2005; 40: 213–227.
[15] Horgan, CO, and Saccomandi, G. A new constitutive theory for fiber-reinforced incompressible nonlinearly elastic solids. *Journal of the Mechanics and Physics of Solids* 2005; 53: 1985–2015.
[16] Guo, ZY, Peng, XQ, and Moran, B. Mechanical response of neo-Hookean fiber-reinforced incompressible nonlinearly elastic solids. *International Journal of Solids and Structures* 2007; 44: 1949–1969.
[17] Kassianidis, F, Merodio, J, Ogden, RW, and Pence, TJ. Azimuthal shear of a transversely isotropic elastic solid. *Mathematics and Mechanics of Solids* 2008; 13: 690–724.
[18] Baek, S, and Pence, TJ. Emergence and disappearance of fiber kinking surfaces in transversely isotropic hyperelastic materials. *ZAMP* 2010; 61: 745–772.
[19] Guo, ZY, Peng, XQ, and Moran, B. A composites-based hyperelastic constitutive model for soft tissue with application to the human annulus fibrosis. *Journal of the Mechanics and Physics of Solids* 2006; 54: 1952–1971.
[20] Hariton, L, deBotton, G, Gasser, TC, and Holzapfel, GA. Stress-driven collagen fiber remodeling in arterial walls. *Biomechanics and Modeling in Mechanobiology* 2007; 6: 163–175.
[21] Holzapfel, GA, Gasser, TG, and Ogden, RW. Constitutive modeling of arteries. *Proceedings of the Royal Society A* 2010; 466: 1551–1597.
[22] Baek, S, and Srinivasa, AR. Modeling of the pH-sensitive behavior of an ionic gel in the presence of diffusion. *International Journal of Nonlinear Mechanics* 2004; 39: 1301–1318.
[23] Qiu, GY, and Pence, TJ. Remarks on the behavior of simple directionally reinforced incompressible nonlinearly elastic solids. *Journal of Elasticity* 1997; 49: 1–30.
[24] Agrawal, CM, and Ray, RB. Biodegradable polymer scaffolds for musculoskeletal tissue engineering. *Journal of Biomedical Materials Research* 2001; 55: 141–150.
[25] Li, WJ, Mauck, RL, Cooper, JA, Yuan, X, and Tuan, RS. Engineering controllable anisotropy in electrospun biodegradable nanotibrous scaffolds for musculoskeletal tissue engineering. *Journal of Biomechanics* 2007; 40: 1686–1693.
[26] Middleton, JC, and Tipton, AJ. Synthetic biodegradable polymers as orthopedic devices. *Biomaterials* 2000; 21: 2335–2346.
[27] Lendlein, A, and Langer, R. Biodegradable, elastic shape-memory polymers for potential biomedical applications. *Science* 2002; 296: 1673–1676.
[28] Sinha, VR, and Trehan, A. Biodegradable microspheres for protein delivery. *Journal of Controlled Release* 2003; 90: 261–280.
[29] Soppimath, KS, Aminabhavi, TM, Kulkarni, AR and Rudzinski, WE. Biodegradable polymeric nanoparticles as drug delivery devices. *Journal of Controlled Release* 2001; 70: 1–20.
[30] Boudriot, U, Dersch, R, Griner, A, and Wendorff, JH. Electrospinning approaches towards scaffold engineering—A brief overview. *Artificial Organs* 2006; 30: 785–792.
[31] Murugan, R, and Ramakrishna, S. Design strategies of tissue engineering scaffolds with controlled fiber orientation. *Tissue Engineering* 2007; 13: 1845–1866.